(U)

SECURITY CLASSIFICATION OF THIS PAGE

(2)

REPORT DOC

AD-A227 307

1a. REPORT SECURITY CLASSIFICATION
Nonclassified

2a. SECURITY CLASSIFICATION AUTHORITY

2b. DECLASSIFICATION/DOWNGRADING SCHEDULE

DTIC ELECTE SEP 26 1990 D CS

3. DISTRIBUTION/AVAILABILITY OF REPORT
Approved for public release, distribution unlimited

4. PERFORMING ORGANIZATION REPORT NUMBER(S)

5. MONITORING ORGANIZATION REPORT NUMBER(S)
AFOSR-TR- 90 0937

6a. NAME OF PERFORMING ORGANIZATION
University of Utah

6b. OFFICE SYMBOL (If applicable)

7a. NAME OF MONITORING ORGANIZATION
AFOSR/Lt. Col. G. K. Haritos

6c. ADDRESS (City, State and ZIP Code)
Department of Mechanical Engineering
Salt Lake City, UT 84112

7b. ADDRESS (City, State and ZIP Code)
Bolling Air Force Base
Washington DC, 20332-6448

8a. NAME OF FUNDING/SPONSORING ORGANIZATION
AFOSR

8b. OFFICE SYMBOL (If applicable)
NA

9. PROCUREMENT INSTRUMENT IDENTIFICATION NUMBER
Grant AFOSR-87-0204

8c. ADDRESS (City, State and ZIP Code)
Bolling Air Force Base
Washington DC, 20332-6448

10 SOURCE OF FUNDING NOS.

PROGRAM ELEMENT NO.	PROJECT NO.	TASK NO.	WORK UNIT NO
61102F	2302	B2	

11. TITLE (Include Security Classification) Failure in Laminated Composite Plates Containing A Hole (U)

12. PERSONAL AUTHOR(S)
E. S. Folias

13a. TYPE OF REPORT	13b. TIME COVERED	14. DATE OF REPORT (Yr., Mo., Day)	15. PAGE COUNT
Final	FROM 87 TO 90	July 25, 1990	

16. SUPPLEMENTARY NOTATION

17 COSATI CODES			18. SUBJECT TERMS (Continue on reverse if necessary and identify by block number)
FIELD	GROUP	SUB. GR.	
			Composite, Plates, Laminates, 3D Analysis

19. ABSTRACT (Continue on reverse if necessary and identify by block number)

It was found convenient for development and clarity purposes to divide the contents of this report in two parts. Part I deals with the 3D stresses in a laminated composite plate weakened by a circular hole. The analysis is based on 3D macromechanical considerations. ~~Part II deals with~~ the debonding aspects between a fiber/matrix interface particularly in the region where the fiber intersects a free edge, e.g. the surface of a hole. The latter results, which are based on micromechanical considerations, are then used ~~in conjunction with the results of part I~~ to predict the critical applied load stress which may cause initiation of ply-delamination. Keywords: Composite Plates; Laminates. (RH)

over

20. DISTRIBUTION/AVAILABILITY OF ABSTRACT
UNCLASSIFIED/UNLIMITED ☒ SAME AS RPT. ☐ DTIC USERS ☐

21. ABSTRACT SECURITY CLASSIFICATION
(U)

22a. NAME OF RESPONSIBLE INDIVIDUAL	22b. TELEPHONE NUMBER (Include Area Code)	22c. OFFICE SYMBOL
~~E. S. Folias~~ GEORGE K. HARITOS, LT. COL. USAF	~~(801) 581-8452~~ (202) 767-4987	NA

DD FORM 1473, 83 APR EDITION OF 1 JAN 73 IS OBSOLETE.

19

SECURITY CLASSIFICATION OF THIS PAGE
(U)

Part I

An eigenfunction expansion is developed for the determination of the exact 3D stress field in the neighborhood of the intersection of the free edge of a hole and an interface in a laminated composite plate. For transversely isotropic laminae, the stress field is shown to possess a weak singularity whose strength depends on the material constants, the fiber orientations of the two adjacent laminae as well as the polar angle θ. Results for $[0°/90°]$, $[0°/70°]$, $[0°/45°]$ and $[0°/2$ are presented and the best and worst fiber orientations are identified.

Finally, the interlaminar stresses are computed and the variation as a function of the angle θ is identified. The circumferential stress $\sigma_{\theta\theta}$ is shown to posses a small jump across the interface. Results for its behavior in the interior of each layer are also given.

Part II

This part deals with the 3D stress field of a cylindrical fiber which is embedded into a resin matrix. The composite is then subjected to a uniform tensile load σ_0. The strain energy release rate is computed and the criterion is used to predict debonding initiation at the fiber/matrix interface. The analysis shows that this failure is most likely to occur at the free surface, ie the region where the fiber intersects a free surface for example a hole, an edge, or a crack. Moreover, it will occur at approximately (1/10) the load value required for the same failure to commense at the center of the fiber length.

The results are also extended to include a doubly periodic array of fibers which are embedded into a matrix. Based on 3D considerations, the stiffness matrix is shown to increase as the volume fraction of the fibers increases. Similarly, the stress σ_{rr} in the matrix is shown to decrease as the volume fraction of the fibers increases.

FINAL REPORT
ON

FAILURE IN LAMINATED COMPOSITE PLATES CONTAINING A HOLE

by

E.S.Folias
Principal Investigator

Submitted to the
Air Force Office of Scientific Research
Bolling Air Force Base, D.C. 20332-6448

AFOSR-87-0204

University of Utah
Salt Lake City UT 84112

FINAL REPORT
ON

FAILURE IN LAMINATED COMPOSITE PLATES CONTAINING A HOLE

by

E.S.Folias
Principal Investigator

Submitted to the
Air Force Office of Scientific Research
Bolling Air Force Base, D.C. 20332-6448

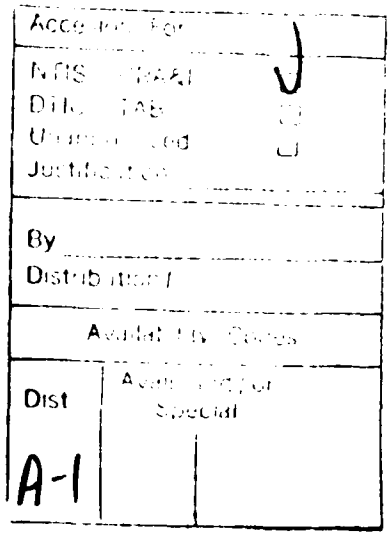

University of Utah
Salt Lake City UT 84112

PREFACE

It was found convenient for development and clarity purposes to divide the contents of this report in two parts. Part I deals with the 3D stresses in a laminated composite plate weakened by a circular hole. The analysis is based on 3D macromechanical considerations. Part II deals with the debonding aspects between a fiber/matrix interface particularly in the region where the fiber intersects a free edge, e.g. the surface of a hole. The latter results, which are based on micromechanical considerations, are then used in conjunction with the results of part I to predict the critical applied load stress which may cause initiation of ply delamination.

Part I

THE 3D STRESS FIELD ADJACENT TO A HOLE IN A LAMINATED COMPOSITE PLATE

Abstract

An eigenfunction expansion is developed for the determination of the exact 3D stress field in the neighborhood of the intersection of the free edge of a hole and an interface in a laminated composite plate. For transversely isotropic laminae, the stress field is shown to possess a weak singularity whose strength depends on the material constants, the fiber orientations of the two adjacent laminae as well as the polar angle θ. Results for [0°/90°], [0°/70°], [0°/45°], and [0°/20°] are presented and the best and worst fiber orientations are identified.

Finally, the interlaminar stresses are computed and the variation as a function of the angle θ is identified. The circumferential stress $\sigma_{\theta\theta}$ is shown to posses a small jump across the interface. Results for its behavior in the interior of each layer are also given.

1 Introduction

Despite careful design, practically every structure contains stress concentrations due to holes. Bolt holes and rivet holes are necessary components for structural joints. It is not surprising, therefore, that the majority of service cracks nucleate in the visinity of a hole. While the subject of stress concentrations is certainly familiar to engineers, the situation is significantly *more* complex in the case of high performance laminated composite materials. The presence of a hole in the laminate introduces significant stress contributions in the third dimension which create a very complicated 3D stress feild in the vicinity of the hole. Moreover, this complex state of stress may depend on the stacking sequence of the laminate, the fiber orientation of each lamina as well as the material properties of the fiber and of the matrix. Ultimately, these stress concentrations form a primary source of damage initiation and property degradation particularly in the presence of cyclic loadings. Recent experimental investigations carried out by Bakis et. al (1986) on graphite epoxy laminates which have been weakened by a circular hole give us a better insight of this damage growth development under the action of cyclic loadings. In general, the progression of this damaged process may be characterized as (i) debonding along fiber-matrix interfaces (ii) matrix cracking parallel to the fibers (iii) matrix cracking between fibers (iv) delamination along the interface of two adjacent laminae with different fiber orientations and (v) fiber breakage.

Thus, if *rational* designs using fiber reinforced-resin matrix composite laminates are to be made, their performance under static, dynamic, fatigue and environmental loads need to be predicatable. The first step towards this goal is the realization that the ultimate failure, as well as many other aspects of the composite behavior, is the result of the growth and accumulation of micro-damage to the fibers, matrix and their interfaces. Thus, it appears that any generally successful model of performance and failure must incorporate the effects of this damage in some way. This certainly represents a challenge.

Delamination has long been recognized as one of the most important failure modes in laminated composite structures. The growth of a delamination may result in a substantial reduction of strength and stiffness of the laminate. The identification, therefore, of such locations in a composite structure is of great interest to the designer. Experimental studies by

Pipes et. al. (1973) have shown that the delamination mode of failure is most likely to initiate at the free edges. One conjectures, therefore, that the stresses at the intersection between a free edge and an interface may well be singular. Indeed, recent analytical investigations (Wang et. al., 1982, and Zwiers e. al. 1982) on straight free edges show that a stress singularity exists there for certain types of laminates.

Alternatively, a curved free edge is inherently a three-dimensional problem which presents greater mathematical difficulties. For this reason, past analyses have been based primarily on finite element methods with standard finite elements (Raju et. al. 1982) as well as elements which incorporate the stress singularity in the formulation (Rybicki et. al. 1978, Ericson et. al. (1984). While such methods can provide us with stress trends in the boundary layer region, it is rather difficult to extract from them with certainty the order of the prevailing stress singularily which is present at the material interface. Moreover, experimental investigations carried out on straight edges (Pagano, 1974) show that the laminate stacking sequence can effect the static strength of the laminates. Similar experimental observations were also made by Daniel et. al (1974) on plates with circular holes. The subject, therefore, does warrant further investigation.

Recently, the author investigated analytically the interliminar stresses at the boundary layer of a hole free-edge but for two isotropic materials of different material constants (Folias 1988). The analysis showed that the stress field there possesses a weak[1] singularity, which singularity depends only on the material properties. In this paper, the author extends this analysis to also include transversely isotropic laminae with a $[0^\circ/90^\circ]$, $[0^\circ/45^\circ]$ as well as other stacking sequences.

2 Formulation of the Problem

Consider the equilibrium of a laminated composite plate which occupies the space $|x| < \infty$, $|y| < \infty$ and $|z| \leq 2h$ and contains a cylindrical hole of radius a whose generators are perpendicular to the bounding planes, namely $z = \pm 2h$. The plate consists of laminae made of transversely isotropic material with a $0^\circ/90^\circ/90^\circ/0^\circ$ stacking sequence. Let the plate be subjected

[1] less than 0.33

to a uniform tensile load σ_0 along the y–axis and parallel to the bounding planes (see Fig. 1).

In the absence of body forces, the coupled differential equations governing the displacement functions u, v, and w are

$$C_{11}\frac{\partial^2 u}{\partial x^2} + C_{66}\frac{\partial^2 u}{\partial y^2} + C_{55}\frac{\partial^2 u}{\partial z^2} + (C_{12}+C_{66})\frac{\partial^2 v}{\partial x \partial y} + (C_{13}+C_{55})\frac{\partial^2 w}{\partial x \partial z} = 0 \tag{1}$$

$$(C_{21}+C_{66})\frac{\partial^2 u}{\partial x \partial y} + C_{66}\frac{\partial^2 v}{\partial x^2} + C_{22}\frac{\partial^2 v}{\partial y^2} + C_{44}\frac{\partial^2 v}{\partial z^2} + (C_{23}+C_{44})\frac{\partial^2 w}{\partial y \partial z} = 0 \tag{2}$$

$$(C_{31}+C_{55})\frac{\partial^2 u}{\partial x \partial z} + (C_{32}+C_{44})\frac{\partial^2 v}{\partial x \partial z} + C_{55}\frac{\partial^2 w}{\partial x^2} + C_{44}\frac{\partial^2 w}{\partial y^2} + C_{33}\frac{\partial^2 x}{\partial z^2} = 0. \tag{3}$$

where the C_{ij}'s are the material constants defining a layer which has its fibers running parallel to the x–axis. For the next layer, the fibers will be running parallel to the y–axis and the governing equations will be obtained from the above by simply interchanging the appropriate coordinates.

The stress–displacement relations for the latyer are given by the constitutive relations

$$\begin{bmatrix} \sigma_{xx} \\ \sigma_{yy} \\ \sigma_{zz} \\ \tau_{yz} \\ \tau_{xz} \\ \tau_{xy} \end{bmatrix} = \begin{bmatrix} C_{11} & C_{12} & C_{13} & 0 & 0 & 0 \\ C_{21} & C_{22} & C_{23} & 0 & 0 & 0 \\ C_{31} & C_{32} & C_{33} & 0 & 0 & 0 \\ 0 & 0 & 0 & C_{44} & 0 & 0 \\ 0 & 0 & 0 & 0 & C_{55} & 0 \\ 0 & 0 & 0 & 0 & 0 & C_{66} \end{bmatrix} \begin{bmatrix} \epsilon_{xx} \\ \epsilon_{yy} \\ \epsilon_{zz} \\ 2\epsilon_{yz} \\ 2\epsilon_{xz} \\ 2\epsilon_{xy} \end{bmatrix} \tag{4}$$

As to boundary conditions, we require that:

$$\text{at} \quad z = \pm 2h: \quad \text{the surface stresses must vanish} \tag{5}$$

at $z = \pm h$: the displacements and surface stresses must match (6)

at $r = a$: the surface stresses must vanish. (7)

Finally, in order to complete the formulation of the problem, the loading conditions far away from the hole must be satisfied.

3 Asymptotic Solution at the Interface

The main objective of this analysis is to derive an asymptotic solution for the 3D stress field in the immediate vicinity of the region where the interface between two laminae meets the free-of-stress surface of the hole. Thus, guided by a general analytical solution for the equilibrium of a linear elastic isotropic layer which the author has recently constructed, we assume the complementary displacement field to be of the form

(i) for lamina [0°]

$$u^{(1)} = \sin\theta \left\{ \ell_{11} \frac{\partial^2}{\partial (r-a)^2} + \ell_{12} \frac{\partial^2}{\partial (h-z)^2} \right\} \frac{\partial^3 H}{\partial (r-a) \partial (h-z)^2} \quad (8)$$

$$v^{(1)} = \cos\theta \left\{ \ell_{21} \frac{\partial^2}{\partial (r-a)^2} + \ell_{22} \frac{\partial^2}{\partial (h-z)^2} \right\} \frac{\partial^3 H}{\partial (r-a) \partial (h-z)^2} \quad (9)$$

$$w^{(1)} = \left\{ \ell_{31} \frac{\partial^4}{\partial (r-a)^4} + \ell_{32} \frac{\partial^4}{\partial (r-a)^2 \partial (h-z)^2} + \ell_{33} \frac{\partial^4}{\partial (h-z)^4} \right\} \frac{\partial H}{\partial (h-z)} \quad (10)$$

where

$$\ell_{11} = -(C_{13}+C_{55})\left[C_{66}\sin^2\theta + C_{22}\cos^2\theta\right]+(C_{12}+C_{66})(C_{23}-C_{44})\cos^2\theta \tag{11}$$

$$\ell_{12} = -(C_{13}+C_{55})C_{44} \tag{12}$$

$$\ell_{21} = (C_{13}+C_{55})(C_{21}+C_{66})\sin^2\theta - (C_{23}+C_{44})(C_{11}\sin^2\theta + C_{66}\cos^2\theta) \tag{13}$$

$$\ell_{22} = -(C_{23}+C_{44})C_{55} \tag{14}$$

$$\ell_{31} = (C_{11}\sin^2\theta + C_{66}\cos^2\theta)(C_{66}\sin^2\theta + C_{22}\cos^2\theta) - \frac{1}{4}(C_{12}+C_{66})^2\sin^2(2\theta) \tag{15}$$

$$\ell_{32} = C_{44}(C_{11}\sin^2\theta + C_{66}\cos^2\theta) + C_{55}(C_{66}\sin^2\theta + C_{22}\cos^2\theta) \tag{16}$$

$$\ell_{33} = C_{44}C_{55}. \tag{17}$$

In writing the above displacements, we used a cylindrical coordinate system and, furthermore, assumed that $(r-a) << a$. In view of the above, one, by direct substitution, can show that the governing equations (1)-(3) are indeed satisfied provided the unknown function H satisfies the differential relation

$$\left[\frac{\partial^2}{\partial(r-a)^2} + \epsilon_1\frac{\partial^2}{\partial(h-z)^2}\right]\left[\frac{\partial^2}{\partial(r-a)^2} + \epsilon_2\frac{\partial^2}{\partial(h-z)^2}\right] \cdot \left[\frac{\partial^2}{\partial(r-a)^2} + \epsilon_3\frac{\partial^2}{\partial(h-z)^2}\right] H = 0, \tag{18}$$

where the ϵ_1, ϵ_2 and ϵ_3 are functions of C_{ij} and θ and represent the roots of the cubic equation

$$\epsilon^3 - \frac{T_2}{T_1}\epsilon^2 + \frac{T_3}{T_1}\epsilon - \frac{T_4}{T_1} = 0. \tag{19}$$

with

$$\begin{aligned} T_1 &= (C_{11}\sin^2\theta + C_{66}\cos^2\theta)(C_{66}\sin^2\theta + C_{22}\cos^2\theta)(C_{55}\sin^2\theta + C_{44}\cos^2\theta) \\ &\quad -\frac{1}{4}(C_{12}+C_{66})^2(C_{55}\sin^2\theta + C_{44}\cos^2\theta)\sin^2(2\theta) \end{aligned} \tag{20}$$

$$\begin{aligned} T_2 &= (C_{11}\sin^2\theta + C_{66}\cos^2\theta)\left[C_{33}(C_{66}\sin^2\theta + C_{22}\cos^2\theta) + \right. \\ &\quad \left. + C_{44}(C_{55}\sin^2\theta + C_{44}\cos^2\theta) - (C_{23}+C_{44})^2\cos^2\theta\right] \\ &\quad +(C_{12}+C_{66})\left[2(C_{23}+C_{44})(C_{31}+C_{55})\sin^2\theta - (C_{21}+C_{66})C_{33}\sin^2\theta\cos^2\theta\right. \\ &\quad \left. -(C_{13}+C_{55})^2(C_{66}\sin^2\theta + C_{22}\cos^2\theta)\sin^2\theta \right. \\ &\quad \left. +C_{55}(C_{66}\sin^2\theta + C_{22}\cos^2\theta)(C_{55}\sin^2\theta + C_{44}\cos^2\theta)\right] \end{aligned} \tag{21}$$

$$\begin{aligned} T_3 &= C_{55}\left[C_{33}(C_{66}\sin^2\theta + C_{22}\cos^2\theta) + C_{44}(C_{55}\sin^2\theta + C_{44}\cos^2\theta)\right. \\ &\quad \left. -(C_{23}+C_{44})^2\cos^2\theta\right] - (C_{13}+C_{55})^2 C_{44}\sin^2\theta \\ &\quad + \left[C_{11}\sin^2\theta + C_{66}\cos^2\theta\right] C_{33}C_{44} \end{aligned} \tag{22}$$

$$T_4 = C_{33}C_{44}C_{55} \tag{23}$$

(ii) for lamina [90°]

$$u^{(2)} = \sin\theta \left\{ \tilde{\ell}_{11} \frac{\partial^2}{\partial(r-a)^2} + \tilde{\ell}_{12} \frac{\partial^2}{\partial(h-z)^2} \right\} \frac{\partial^3 \tilde{H}}{\partial(r-a)\partial(h-z)^2} \quad (24)$$

$$v^{(2)} = \cos\theta \left\{ \tilde{\ell}_{21} \frac{\partial^2}{\partial(r-a)^2} + \tilde{\ell}_{22} \frac{\partial^2}{\partial(h-z)^2} \right\} \frac{\partial^3 \tilde{H}}{\partial(r-a)\partial(h-z)^2} \quad (25)$$

$$w^{(2)} = \left\{ \tilde{\ell}_{31} \frac{\partial^4}{\partial(r-a)^4} + \tilde{\ell}_{32} \frac{\partial^4}{\partial(r-a)^2\partial(h-z)^2} + \tilde{\ell}_{33} \frac{\partial^4}{\partial(h-z)^4} \right\} \frac{\partial \tilde{H}}{\partial(h-z)} \quad (26)$$

$$\tilde{\ell}_{11} = -(C_{23}+C_{44})[C_{66}\sin^2\theta + C_{11}\cos^2\theta] + (C_{12}+C_{66})(C_{13}+C_{55})\cos^2\theta \quad (27)$$

$$\tilde{\ell}_{12} = -(C_{23}+C_{44})C_{55} \quad (28)$$

$$\tilde{\ell}_{21} = \left\{ C_{23}+C_{44})(C_{21}+C_{66})\sin^2\theta - (C_{13}+C_{55})(C_{22}\sin^2\theta + C_{55}\cos^2\theta) \right\} \quad (29)$$

$$\tilde{\ell}_{22} = -(C_{13}+C_{55})C_{44} \quad (30)$$

$$\tilde{\ell}_{31} = (C_{22}\sin^2\theta + C_{66}\cos^2\theta)(C_{66}\sin^2\theta + C_{11}\cos^2\theta) - (C_{12}+C_{66})^2\sin^2\theta\cos^2\theta \quad (31)$$

$$\tilde{\ell}_{32} = C_{55}(C_{22}\sin^2\theta + C_{66}\cos^2\theta) + C_{44}(C_{66}\sin^2\theta + C_{11}\cos^2\theta) \quad (32)$$

$$\tilde{C}_{33} = C_{44}C_{55}, \tag{33}$$

and the function $\tilde{H}(r-a, h-z)$ is of the same form as the H of layer $[0^\circ]$, except that ϵ_1, ϵ_2, ϵ_3 are now replaced by the appropriate $\tilde{\epsilon}_1$, $\tilde{\epsilon}_2$, $\tilde{\epsilon}_3$ of layer $[90^\circ]$.

It remains, therefore, for us to construct a solution to equation (18). To accomplish this, we introduce the local, to the corner, stretched coordinate system (see Fig. 2), i.e.

$$r - a = \rho\cos\phi \tag{34}$$

$$\frac{(h-z)}{\sqrt{\epsilon_1}} = \rho\sin\phi. \tag{35}$$

Omitting the long and tedious mathemataical details, the solution to equation (18), in terms of the local coordinates, is found to be

$$H(\rho,\phi) = \rho^\alpha \left\{ A_1\cos(\alpha\phi) + B_1\sin(\alpha\phi) + \frac{1}{\alpha}\int_0^\phi \psi_1(\xi)\sin[\alpha(\phi-\xi)]\,d\xi \right\} + (\rho^{\alpha+1}) \tag{36}$$

where

$$\psi_1(\phi) = \{A_2\cos[(\alpha-2)\tan^{-1}\phi_2] + B_2\sin[(\alpha-2)\tan^{-1}\phi_2]\} + \frac{1}{(\alpha-2)}\int_0^{\phi_2}\psi_2(\xi)\sin[(\alpha-2)(\phi_2-\xi)]\,d\xi\,\}\left(\frac{\rho_2}{\rho}\right)^{\alpha-2}, \tag{37}$$

$$\frac{\rho_2}{\rho} = \frac{\sqrt{1+\dfrac{\epsilon_1}{\epsilon_2}\tan^2\phi}}{\sqrt{1+\tan^2\phi}}, \tag{38}$$

$$v_2(\phi_2) = \left(\frac{\rho_3}{\rho_2}\right)^{\alpha-4} \quad \{ A_3 \cos\left[(\alpha-4)\tan^{-1}\left(\sqrt{\frac{\epsilon_2}{\epsilon_3}}\tan\phi_2\right)\right] \tag{39}$$

$$+B_3 \sin\left[(\alpha-4)\tan^{-1}\left(\sqrt{\frac{\epsilon_2}{\epsilon_3}}\tan\phi_2\right)\right] \} .$$

$$\left(\frac{\rho_3}{\rho_2}\right) = \sqrt{\frac{1+\frac{\epsilon_2}{\epsilon_3}\tan^2\phi_2}{1+\tan^2\phi_2}} \tag{40}$$

$$\phi_2 = \tan^{-1}\left(\sqrt{\frac{\epsilon_1}{\epsilon_2}}\tan\phi\right) . \tag{41}$$

and α, A_i and $B_i (i = 1,2,3)$ are constants to be determined from the boundary conditions.

Substituting the previously constructed displacement field into the boundary conditions:

at $\phi = 0$:

$$u^{(1)} = u^{(2)} \tag{42}$$

$$v^{(1)} = v^{(2)} \tag{43}$$

$$w^{(1)} = w^{(2)} \tag{44}$$

$$\sigma_{zz}^{(1)} = \sigma_{zz}^{(2)} \tag{45}$$

$$\tau_{xz}^{(1)} = \tau_{xz}^{(2)} \tag{46}$$

$$\tau_{yz}^{(1)} = \tau_{yz}^{(2)} \tag{47}$$

at $\phi = -\frac{\pi}{2}$:

$$\sigma_{rr}^{(1)} = 0 \tag{48}$$

$$\tau_{r\theta}^{(1)} = 0 \tag{49}$$

$$\tau_{rz}^{(1)} = 0 \tag{50}$$

at $\phi = \dfrac{\pi}{2}$:

$$\sigma_{rr}^{(2)} = 0 \tag{51}$$

$$\tau_{r\theta}^{(2)} = 0 \tag{52}$$

$$\tau_{rz}^{(2)} = 0 \tag{53}$$

we arrive at a system of twelve algebraic equations, the determinant of which must vanish. This latter condition leads to the determination of the characteristic values α. In general, the values of α depend on the material constnats C_{ij}, as well as on the angle θ.

4 The Isotropic Case

As a limit check, we let the laminae be homogeneous and isotropic but of different material constants. Without going into the mathematical details, the material constants of lamina 1 become:

$$C_{11} = C_{22} = C_{33} = 2\left(\frac{1-\nu_1}{1-2\nu_1}\right) G_1 \tag{54}$$

$$C_{44} = C_{55} = C_{66} = G \tag{55}$$

$$C_{12} = C_{23} = C_{13} = \frac{2\nu_1}{1-2\nu_1} G_1, \tag{56}$$

in view of which the displacement reduce to:

$$u^{(1)} = \sin\theta \frac{\partial}{\partial(r-a)} \left\{ \frac{G_1}{1-2\nu_1} \left[\frac{\partial^2}{\partial(r-a)^2} + \frac{\partial^2}{\partial(h-z)^2} \right] \right\} \frac{\partial^2 H}{\partial(h-z)^2} \quad (57)$$

$$v^{(1)} = \cos\theta \frac{\partial}{\partial(r-a)} \left\{ \frac{G_1}{1-2\nu_1} \left[\frac{\partial^2}{\partial(r-a)^2} + \frac{\partial^2}{\partial(h-z)^2} \right] \right\} \frac{\partial^2 H}{\partial(h-z)^2} \quad (58)$$

$$w^{(1)} = G_1 \left\{ \frac{\partial^2}{\partial(r-a)^2} + \frac{\partial^2}{\partial(h-z)^2} \right\} \left\{ 2\left(\frac{1-\nu_1}{1-2\nu_1} \right) \frac{\partial^2 H}{\partial(r-a)^2} + \frac{\partial^2 H}{\partial(h-z)^2} \right\}. \quad (59)$$

Notice that the θ-dependence has totally been eliminated and that the function H now attains the very simple form

$$H = \rho^{\alpha} \{ A_1 \cos(\alpha\phi) + B_1 \sin(\alpha\phi) + A_2 \cos(\alpha-2)\phi + B_2 \sin(\alpha-2)\phi + A_3 \cos(\alpha-4)\phi + B_3 \sin(\alpha-4)\phi \} + (\rho^{\alpha+1}). \quad (60)$$

Similarly, the $\tilde{H}$ collapses to the same expression except that the constants A_i and B_i are replaced by $\tilde{A}_i$ and $\tilde{B}_i$ respectively. The numerical results for this case lead to the same results as those recently reported by Folias (1988). Fig. 3, for example, depicts typical values of α.

5 Characterization of the Free–Edge Stress Singularity

Returning next to the algebraic system (42)-(53), if one considers the case of a graphite/epoxy layer, with coefficients C_{ij} (Knight 1982)

$$C_{ij} = \begin{bmatrix} 20.6228 & 1.0381 & 1.0381 & 0.0000 & 0.0000 & 0.0000 \\ 1.0381 & 2.2301 & 1.2301 & 0.0000 & 0.0000 & 0.0000 \\ 1.0381 & 1.2301 & 2.2301 & 0.0000 & 0.0000 & 0.0000 \\ 0.0000 & 0.0000 & 0.0000 & 0.5000 & 0.0000 & 0.0000 \\ 0.0000 & 0.0000 & 0.0000 & 0.0000 & 0.8696 & 0.0000 \\ 0.0000 & 0.0000 & 0.0000 & 0.0000 & 0.0000 & 0.8696 \end{bmatrix}, \quad (61)$$

then the requirement of the determinant of the system to vanish leads to a transcendental equation for the roots α. The only roots of practical interest are those which lie in the interval $5 < Re\ \alpha < 6$. The numerical results for the 12×12 system were carried out in double precision. Omitting the long and tedious numerical details, the values of the characteristic α for $[0^\circ/90^\circ]$, $[0^\circ/70^\circ]$, $[0^\circ/45^\circ]$ and $[0^\circ/20^\circ]$ interfaces[2] are shown in Fig. 4. Two important characteristics are worth mentioning. First, the stress singularity is a funciton of the material constants C_{ij}, the angle of sweep θ and the fiber orientation of the respective laminae. Second, the singularity strength for anisotropic materials appear to be much weaker than that of isotropic materials. The latter may have severe consequences to the damage process and to the reduction of the overall strength in the plate. As a practical matter, if one plots the $\max(\alpha - 6)$ as a function of the fiber angle orientation β for a $[0^\circ/\beta^\circ]$ interface one can identify the most and least desirable fiber orientations. This is depicted in Fig. 5.

Similar stress singularity profiles (see Fig. 4) have also been obtained by Wang et. al. (1982) in their pioneering work on straight edges using a different method of solution. The present analysis complements that and shows that, for sufficiently large holes, the results for curved edges will be the same as those obtained near a straight free edge provided layer orientations in the second problem are properly chosen to reflect the circumpherential position of a point on the hole boundary and the interface. While this result was to be expected, it could not be taken for granted. This is because the latter method represents a descrete, rather than a continuous, approach and the outcome of the limiting process had to be established. Moreover, the present method of solution shows how a 3D analysis can indeed be developed to also include this continuous dependence on the angle θ and thus provide us with further insight on the construction of such 3D solutions to transversely isotropic plates with more complicated flaw geometries.

It may further be noted that the macromechanical approach actually underestimates the value of the stresses at such regions. For example, if we examine the local geometry from a micromechanical point of view, e. g. at $\theta = 0^\circ$ and for a $[0^\circ/90^\circ]$ interface, one notices that the adjacent fiber of layer $[90^\circ]$ intersects the free surface of the hole boundary perpendicularly. The explicit 3D solution for the stress field in such regions is also

[2]The results are presently generalized for an arbitrary $[0/\beta]$ interface.

known. In particular, for a glass fiber embedded into an epoxy matrix the stress singularity is found to be 0.2489 (Folias 1989, Folias 1990a) while for a carbon fiber embedded into an epoxy matrix is found to be 0.2815 (Folias 1990b). The former analysis assumes the fiber to be of an isotropic material while the latter assumes the fiber to be of a transversely isotropic material. Comparing these results with those of Fig. 4 it is clear that the stress singularity predicted by the macromechanical theory is indeed underestimated. Such information becomes essential for the proper estimation of the local damaged zone. This matter will be discussed further later on.

In the case of a $[0^{\circ}/90^{\circ}]$ interface, the profile of the characteristic value α versus θ is symmetric with respect to the line $\theta = 45^{\circ}$. The same behavior was also obtained by Ericson et. al. (1984) by using finite elements. The present results, however, exhibit a stronger singularity than that found in the above reference. The author attributes this to two factors. First the material constants were different and second it is rather difficult to obtain accurate results for the singularity strength based on finite element analyses. On the other hand, it is impressive indeed that Ericson et. al. (1984) as well as Raju et. al (1982) were able to recover the exact profile as a function of θ and the relative magnitude.

In order to make a proper comparision with the results of Ericson et. al., one should use the same material constants, C_{ij}, as those used in the above reference. Computing, therefore, the C_{ij}'s from the data of the above reference (see Appendix), our analysis gives the characteristic values depicted in Fig. 6. At $\theta = 45^{\circ}$, for example, $\alpha = 5.9755$ or $\alpha - 6 = 0.0245$. If we now compare this value with that found by Wang et. al. (1982), for $a \pm 45^{\circ}$ straight edge interface, i.e. $\alpha - 6 = 0.0255$, we see that the comparison is very good. The minor difference is probably due to the small variation of the C_{ij}'s used depending as to how they are computed. Our results are based on the C_{ij}'s shown in the Appendix. The results in the region between $20 < \theta < 80$ compare very well with those reported by Ericson et. al. On the other hand, for $0 \leq \theta \leq 20$, our singularity strength is found to be slightly higher and the characteristic bell shape profile is preserved.

Pagano et. al. (1973) have shown that high tensile σ_{zz} stresses are associated with the decreased laminate strengths reported by Pipes et. al. (1973). This observation points to the importance of understanding the interlaminar stress behavior near free edges in laminates. It is now possible to compute the interlaminar stresses adjacent to the hole surface. In

particular,

$$\sigma_{3i} \sim \rho^{\alpha-6} f_{3i}\left(\theta, \alpha; C_{kl}, \tilde{C}_{mn}\right), \tag{62}$$

where the f_{3i} are rather long and complicated functions of the angles θ and ϕ and the material constants. The plots for σ_{zz}, τ_{rz}, $\tau_{\theta z}$, for a [0 /90] interface, are given in Fig. 7. Notice that the *max* σ_{zz} stress for a [0 /90] interface occurs[3] at $\theta = 23^{\circ}$. The result is in agreement with that found previously based on finite elements (Ericson et. al and Raju et. al.).

The reader may also note that all the stresses are normalized with respect to a function $C(\theta)$ which is negative and may vary slightly as one travels along the direction of θ. This function of *theta* is to be determined from a separate analysis valid across the thickness of the plate by comparing the relative $\sigma_{\delta\theta}$ stress functions. The analysis is presently being completed and will be reported separately. The present analysis, however, does provide us with the relative magnitudes of the interlaminar stresses (see Fig. 8).

The results show the shear stress τ_{rz} to be relatively low throughout. On the other hand, the normal stess σ_{zz} appears to be dominant in the range $-30^{\circ} \leq \theta \leq 30^{\circ}$ beyond which the shear stress $\tau_{\theta z}$ now becomes the controlling stress, i.e. along $30^{\circ} < \theta < 60^{\circ}$ with its maximum occuring at $\theta = 45^{\circ}$. A more clear plot for the stress σ_{zz} at the interface is given in Fig. 9. Finally, Fig. 10 depicts the jump which exists on the stress $\sigma_{\delta\theta}$ as one moves across the interface, i.e. at $\phi = 0^{+}$ and $\phi = 0^{-}$. The maximum difference occurs at $\theta = 0$ and is approximately 27%. In Figs. 11 and 12 we compare the stress $\sigma_{\theta\theta}^{[0]}$ at $\phi = 0-$ and ϕ =-90° and $\sigma_{\theta\theta}^{[90]}$ at $\phi = 0+$ and $\phi = +90^{\circ}$ respectively.

In view of the above, one may draw the following conclusions for a [0/90°] stacking sequence:

(a) In the vicinity of the interface there exists a boundary layer effect where the stress field changes rather abruptly.

(b) The res k of delamination initiation is highest at θ equal to 23°.

[3] The reader should also take into account the fact that $(6-\alpha)$ is a maximum at $\theta = 45^{\circ}$ and that $C(\theta)$ is negative. The results are based on data give by Eq. (61). Also at $\theta = 0$, $C(\theta) \approx -1.05(h)^{6-\alpha}\sigma_0$.

(c) As one moves away from the plane of the interface, the stress concentration factor in layer [90°] decreases rapidly (see region $-20 < \theta < 20$ where debonding along fiber matrix interfaces are most likely to initiate).

(d) Substantial damage is expected to occur in the region $-40^{\circ} < \theta < 40^{\circ}$.

(e) For the given set of material constants C_{ij}, $\alpha - 6$ is maximum at $\theta^{*} = \theta^{*}_{m} \equiv (3/2)$.

(f) In general, the magnitude of the singularity strength depends on the material constants, C_{ij}, and on the fiber orientation of the two respective laminae.

(g) As one moves approximately one radius distance away from the hole surface, the s.c.f. (stress concentartion factor) is expected to decrease to within 10% of the value of the corresponding case of a plate without a hole (Folias 1990 isotropic case).

6 Discussion

Delamination at free-edges has been a problem of significant concern in the design of advanced fiber composites. The separation of the laminae, caused by high local interlaminar stresses and low strength along the laminae interface, may result in ineffective load transfer, reduction in stiffness and ultimately loss of structural integrity. In this study, the problem has been investigated by treating each lamina as a homogeneous, transversely isotropic, material. Thus the micromechanics effects of fiber size are not included, although a few of these effects, eg. when a fiber meets a free surface have been reported separately (Folias, 1989).

The analytical investigation of the 3D stress field adjacent to the hole and in the vicinity of the interfaces of two laminae of [0°/90°], and [0°/45°], and other fiber orientation shows the stresses to be singular, $\sigma_{ij} \sim \rho^{\alpha-6}$. In general, the singularity exponent depends on the material properties, the corresponding fiber orientations as well as the angle of sweep. The results provide us with better insight for the proper understanding of interlaminar stresses and the effect which they have on the mechanism of failure.

For example, for isotropic laminae the stress singularity is a rather weak singularity (< 0.33), while in transversely isotropic laminae it can be of a much higher order (< 0.99) suggesting, therefore, a greater influence in the damage process.

Pagano et. al (1971, 1974) postulated that throughout the thickness it is the stress σ_{zz} which is the main cause of delamination for polymeric based structural composites. This observation was based on experimental as well as analytical evidence for laminates with different stacking sequences. Our analytical results are consistent with this observtion particularly in the region where θ is small. Alternatively, for larger values of θ the shear stress $\tau_{\theta z}$ plays a much more dominant role on interlaminar failures. Moreover, in the case of a $[0^\circ/90^\circ]$ interface delamination is most likely to take place at $\theta = 23^\circ$. The strain energy release rate may now be used in conjunction with the local stress field to predict delamination failures. This matter is presently under investigation.

Finally, one may conclude that it is possible to reduce the likelyhood of the delamination mode of failure and thereby increase the laminate strength. This can be accomplished by carefully considering the effects of the singularity curves, the stress curves, the load direction and the individual fiber orientations at each interface. Moreover, in future applications it may be possible to choose the material constants C_{ij} so that the coefficients of the singular terms of the interlaminar stresses vanish.

7 Micromechanical Considerations

If one examines the region adjacent to the hole and at the vicinity of the interface from a micromechanical point of view one notices the arrangement depicted in Fig. 13(a). More specifically, in one layer the fibers intersect the free surface of the hole perpendicularly, while in the other layer they run tangent to its surface (see Fig. 13b). Locally, however, this represents the problem of a fiber intersecting a free surface and being subjected to a biaxial load normal to the direction of the fiber. As part of this investigation, this problem has been recently studied by the author and the results for the case of an isotropic fiber have been reported in Folias (1989). The explicit local stress field for one fiber may be found in part B of this report. Without going nto the mathematical details, the local stress field was found to be

singular. More specifically, the stresses were shown to be of the form

$$\sigma_{ij} \sim \tilde{\rho}^{(\tilde{\alpha}-2)} \tag{63}$$

where the exponent $\tilde{\alpha}$ in general is a function of the material properties. In the case of a glass fiber embedded into an epoxy matrix with the properties

$$G_f = 35.00GPa \quad \nu_f = 0.22$$

$$G_m = 2.10GPa \quad \nu_m = 0.34$$

the stress singularity strength is found to be equal to $2 - \tilde{\alpha} = 0.2489$. It is well recognized, however, that carbon fibers are transversely isotropic rather than isotropic. For this reason, the previous analysis has been extended to also include a transversely isotropic fiber (Folias and Li 1990). Without going into the mathematical details, the stress singularity for a carbon fiber embedded into an epoxy matrix was found to be slightly higher, i.e. $2 - \tilde{\alpha} = 0.282$.

Comparing these results with those of Fig. 4 (see Fig. 14) it becomes clear that the derived stress field adjacent to the hole based on macromechanical considerations is indeed underestimated. Such information is essential if one is to predict failure initiation and local damage degradation adjacent to the hole.

Thus one may view the process of delamination as the interfacial cracking of the last row of fibers which intersect the free surface of the hole (see Fig. 13b which corresponds to $\theta = 90^{\circ}$, or $\theta = 0$ if the figure in flipped). Recalling the results of the surface displacement of the problem studied by Penado and Folias (1989, see Figs. 14 and 15 of that paper), one concludes that debonding is most likely to take place at the lower side of the fiber, e.g. see Fig. 13b. It would be of great practical interest if one could predict a priori the critical applied stress σ_0 which may cause a fiber/matrix debonding to initiate and subsequently propagate and become a full size delamination crack (see Fig. 7 of Part II). In order to accomplish this, we use the results of part II, in particular equations (29b and 33) and apply them at the position[4] $\theta \approx 0$. Thus

[4]Notice that σ_{zz} is $\approx$ the same for $0 < \theta < 25$.

$$(0.6944)(9.5958)(44\sigma_0)(\frac{a}{h})^{-0.12}\sqrt{2a_f\beta} = 1.8146\sqrt{\gamma_{12}G_m}, \quad (64)$$

where the first term is due to the periodicity of the fibers, the third term is due to the local stress concentration factor, a is the radius of the hole, h is the thickness of the layer, a_f the radius of the fiber, γ_{12} is the surface energy, and G_m the shear modulus of the matrix and 2β the angle of debond. Next, solving for the critical stress σ_0 one finds

$$(\sigma_0)_{cr} \approx 6.189 \times 10^{-3}\sqrt{\frac{\gamma_{12}G_m}{2a_f\beta}}(\frac{h}{a})^{0.12}. \quad (65)$$

Assuming a fiber diameter of $0.001cm$, a matrix shear modulus of $2.1GPa$, and a surface energy of $270J/m^2$ for well-bonded interfaces, one finds

$$(\sigma_0)_{cr} \approx 2.00\frac{1}{\sqrt{2\beta}}(\frac{h}{a})^{0.12}MPa. \quad (66)$$

For Poorly bonded interfaces the constant is approximately one half of that.

Appendix

From Ericson et. al data (1984)

$$E_{11} = 138GPa \qquad E_{22} = E_{33} = 14.5GPa$$

$$G_{12} = G_{13} = G_{23} = 5.9\ GPa$$

$$\nu_{12} = \nu_{13} = \nu_{23} = 0.21,$$

we compute:

$$C_{11} = 139.6381$$

$$C_{12} = 3.9002$$

$$C_{13} = 3.9002$$

$$C_{22} = 15.2779$$

$$C_{23} = 3.2944$$

$$C_{33} = 15.2779$$

$$C_{44} = C_{55} = C_{66} = 5.9$$

in view of which our program then gives:

θ	α
0.1	5.9440
10	5.9469
15	5.9698
20	5.9714
30	5.9739
45	5.9755

REFERENCES

1. Bakis, C. E., and Stinchcomb, W. W., 1986 "Response of Thick, Notched Laminates Subjected to Tension-Compression Cyclic Loads" ASTM STP 907, pp. 314-334.

2. Pipes, R. B., Kaminski, B. E., Pagano, N. T. 1973 "Influence of the Free Edge Upon The Strength of Angle-Ply Laminates" ASTM STP 521, p. 218.

3. Wang, S. S. and Choi, I., 1982 "Boundary-Layer Effects in Composite Laminates: Part I - Free-edge Stress Singularities" J. Appl. Mech., vol. 49, p. 541.

4. Zwiers, R. I., Ting, T.C.T., Spilker, R. L., 1982, "On the Logarithmic Singularity of Free-edge Stress in Laminated Composites Under Uniform Extension", J. Appl. Mech., vol. 49, p. 561.

5. Raju, I.S., Crews, J. H., 1982, "Three-dimensional Analysis of [0, 90]s and [90/0]s Laminates with a Central Circular Hole." Composites Technology Review, vol. 4, p. 116.

6. Rybicki, E. F., Schmueser, D. W., 1978, "Effect of Stacking Sequence and Lay Up Angle on Free Edge Stresses Around a Hole in a Laminated Plate Under Tension" J. of Composite Materials, vol. 12, p. 300.

7. Ericson, K., Persson, M., Carlsson L. and Gustavsson, A., 1984, "On the Prediction of the Initiation of Delamination in a [0/90]s Laminate with a Circular Hole," Journal of Composite Materials, vol. 18.

8. Pagano, N.J., 1974, "On the Calculation of Interlaminar Normal Stress in Composite Laminates" J. Of Composite Materials, vol. 8, p. 89.

9. Daniel, I.M., Rowlands, R. E. and Whiteside, J.B., 1974, "Effects of Material and Stacking Sequence on Behavior of Composite Plates with Holes," Experimental Mechanics, vol. 14, No. 1, p. 1.

10. Folias, E.S., 1988. "On the Interlaminar Stresses of a Composite Plate Around the Neighborhood of a Hole." Int. J. Solids Structures, Vol. 25, No. 10, pp 1193-1200.

11. Folias, E. S., 1990 a. "On the Prediction of Failure at a Fiber/Matrix Interface in a Composite Subjected to a Transverse Tensile Load," submitted for publicatoin to the Journal of Composite Materials.

12. Folias, E. S., and Li, P., 1990 b. "The 3D Stress Field of a Carbon Fiber Embedded Into an Epoxy Matrix and Intersecting a Free Surface," in preparation.

13. Knight, M., 1982, "Three-Dimensional Elastic Moduli of Graphite/Epoxy Composites," J. Composite Materials, vol. 16, p. 153.

14. Folias, E.S., 1989, "On the Stress Singularities at the Intersection of a Cylindrical Inclusion with the Free Surface of a Plate," International Journal of Fracture, vol. 39 pp. 25-34.

15. Pagano, N.J. and Pipes, R. B., 1973 "Some Observations on the Interlaminar Strength of Composite Materials," Int. J. Mechanical Sciences, vol. 15, p. 679.

16. Penado, F. E. and Folias, E.S., 1989, "The Three-Dimensional Stress Field Around a Cylindrical Inclusion in a Plate of Arbitrary Thickness," International Journal of Fracture, vol. 39, pp. 129-146.

FIGURE CAPTIONS

Fig. 1. Laminated plate of arbitrary thickness with a circular hole.

Fig. 2. Definition of local coordinates at the interface.

Fig. 3. Singularity strength for isotropic laminae.

Fig. 4. Singularity strength for transversely isotropic laminae $[0^\circ/90^\circ]$.

Fig. 5. Best and worse fiber orientations.

Fig. 6. Singularity strength for transversely isotropic laminae $[0^\circ/90^\circ]$ based on Ericson et. al. data.

Fig. 7. Interlaminar stresses for a $[0^\circ/90^\circ]$ interface.

Fig. 8. Interlaminar shear stress ratio for a $[0^\circ/90^\circ]$ interface.

Fig. 9. The interlaminar stress σ_{zz} vs θ.

Fig. 10. The stress concentration factor for $\phi = 0^+$ and 0^-.

Fig. 11. The stress $\sigma_{\theta\theta}^{[0]}$ for $\phi = 0^+$ and $\phi = 90^\circ$.

Fig. 12. The stress $\sigma_{\theta\theta}^{[90]}$ for $\phi = 0^-$ and $\phi = -90^\circ$.

Fig. 13. (a) Geometrical representation.

(b) Local geometry based on micromechanical considerations. (Position $\theta = 90^\circ$)

Fig. 14. Comparison of stress singularities.

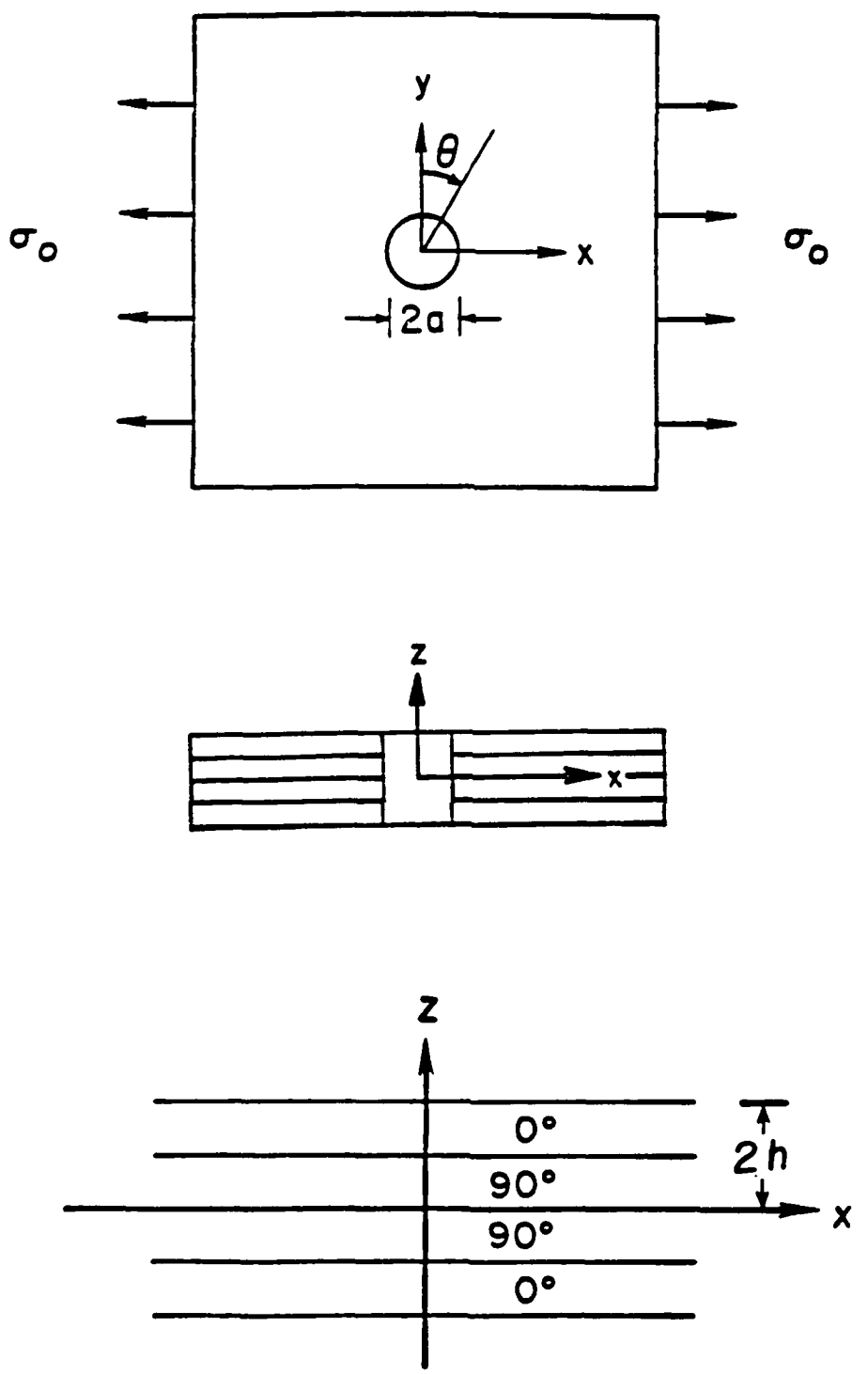

Fig. 1. Laminated plate of arbitrary thickness with a circular hole.

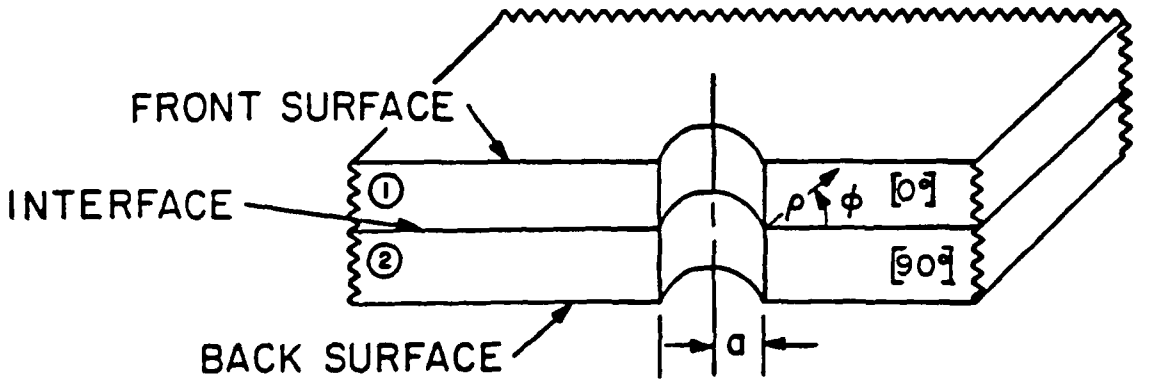

Fig. 2. Definition of local coordinates at the interface.

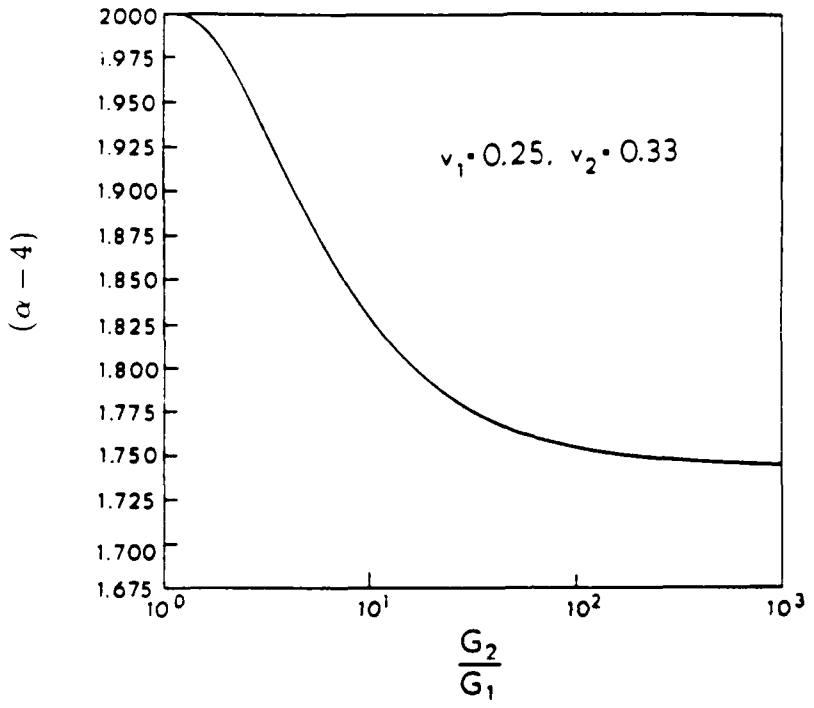

Fig. 3. Singularity strength for isotropic laminae.

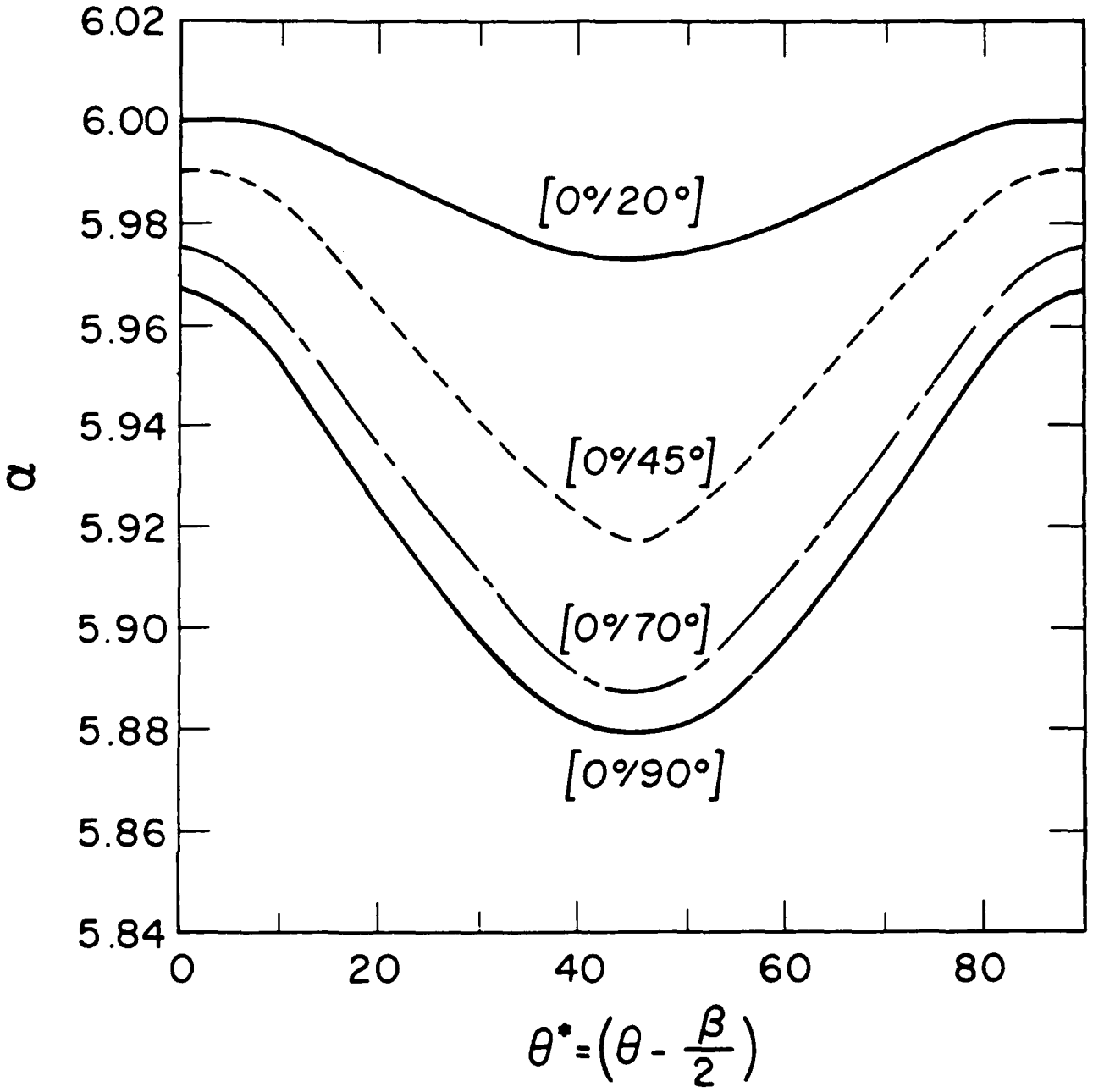

Fig. 4. Singularity strength for transversely isotropic laminae [0°/90°].

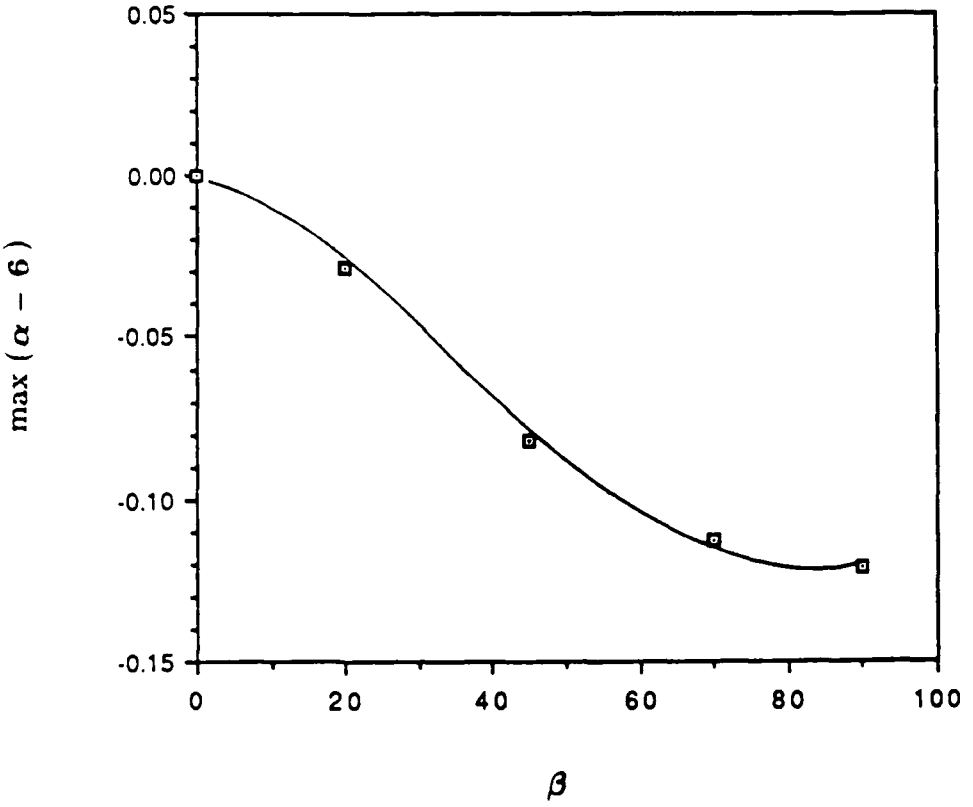

Fig. 5. Best and worse fiber orientations.

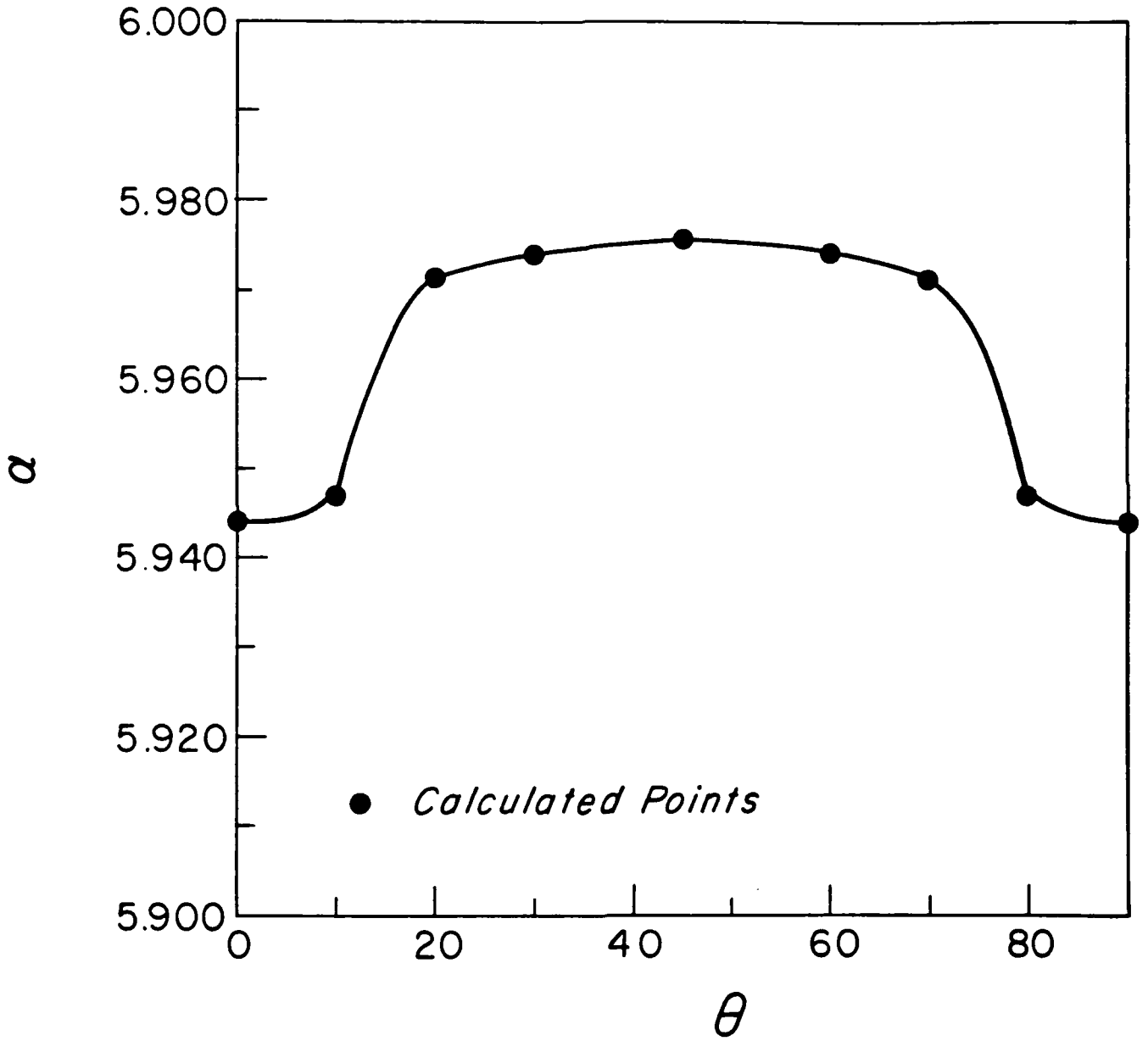

Fig. 6. Singularity strength for transversely isotropic laminae [0°/90°] based on Ericson et. al. data.

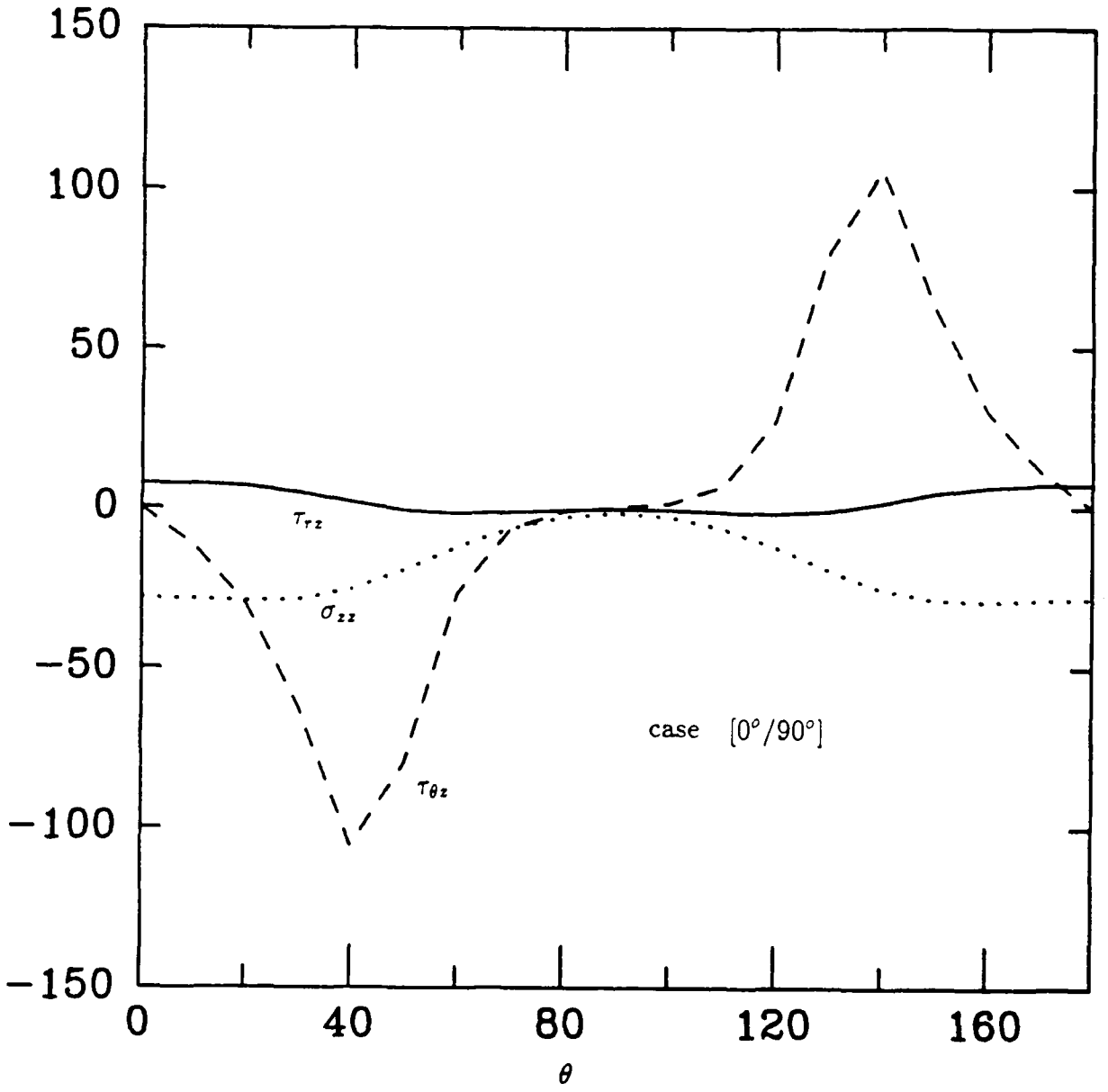

Fig. 7. Interlaminar stresses for a [0°/90°] interface.

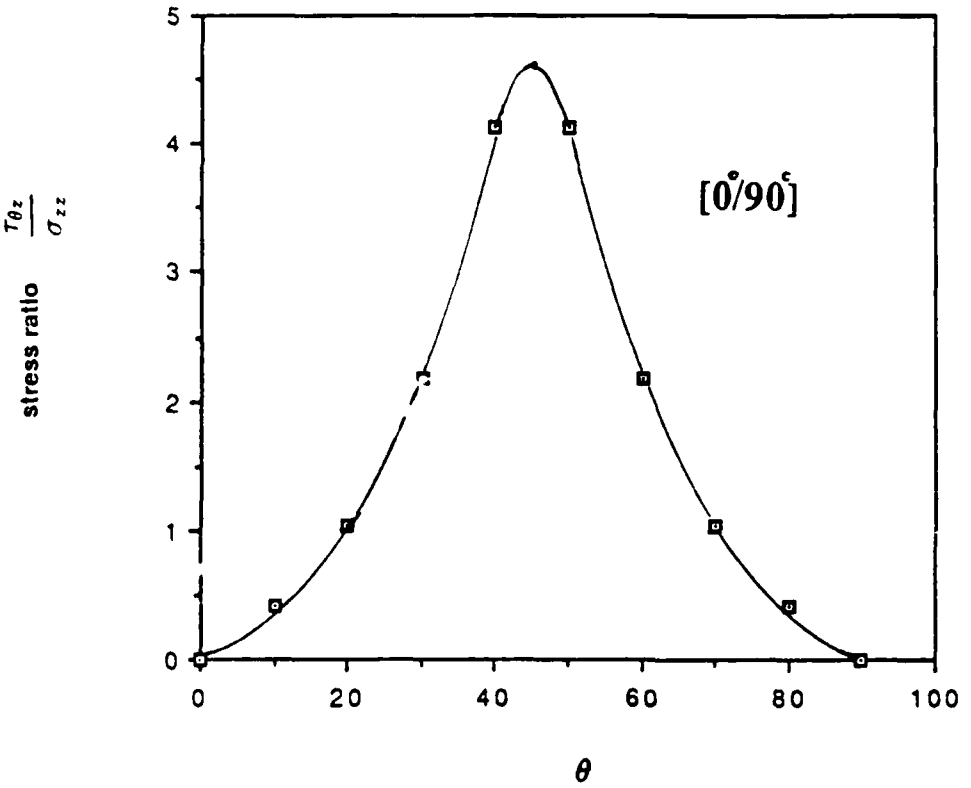

Fig. 8. Interlaminar shear stress ratio for a [0°/90°] interface.

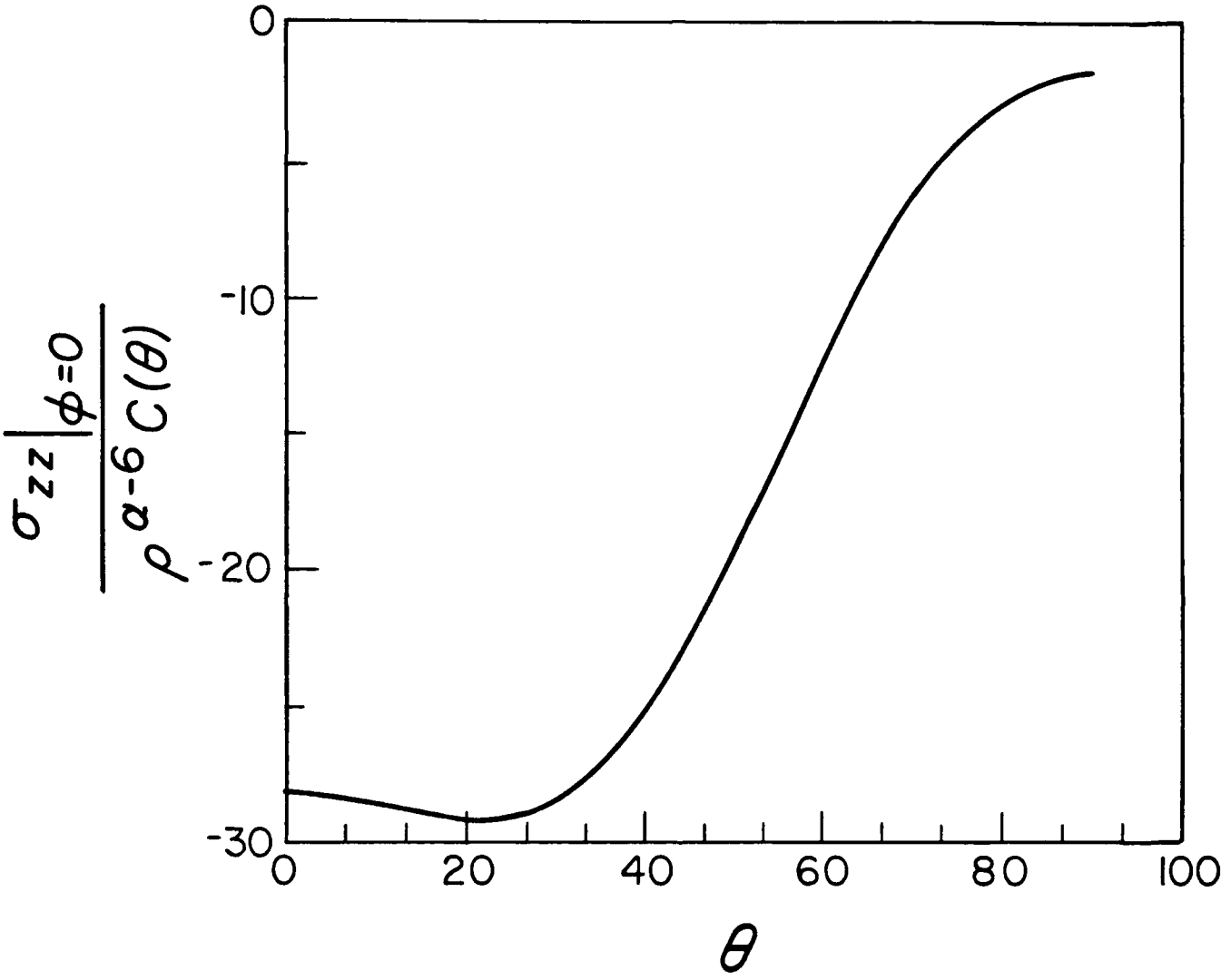

Fig. 9. The interlaminar stress σ_{zz} vs θ.

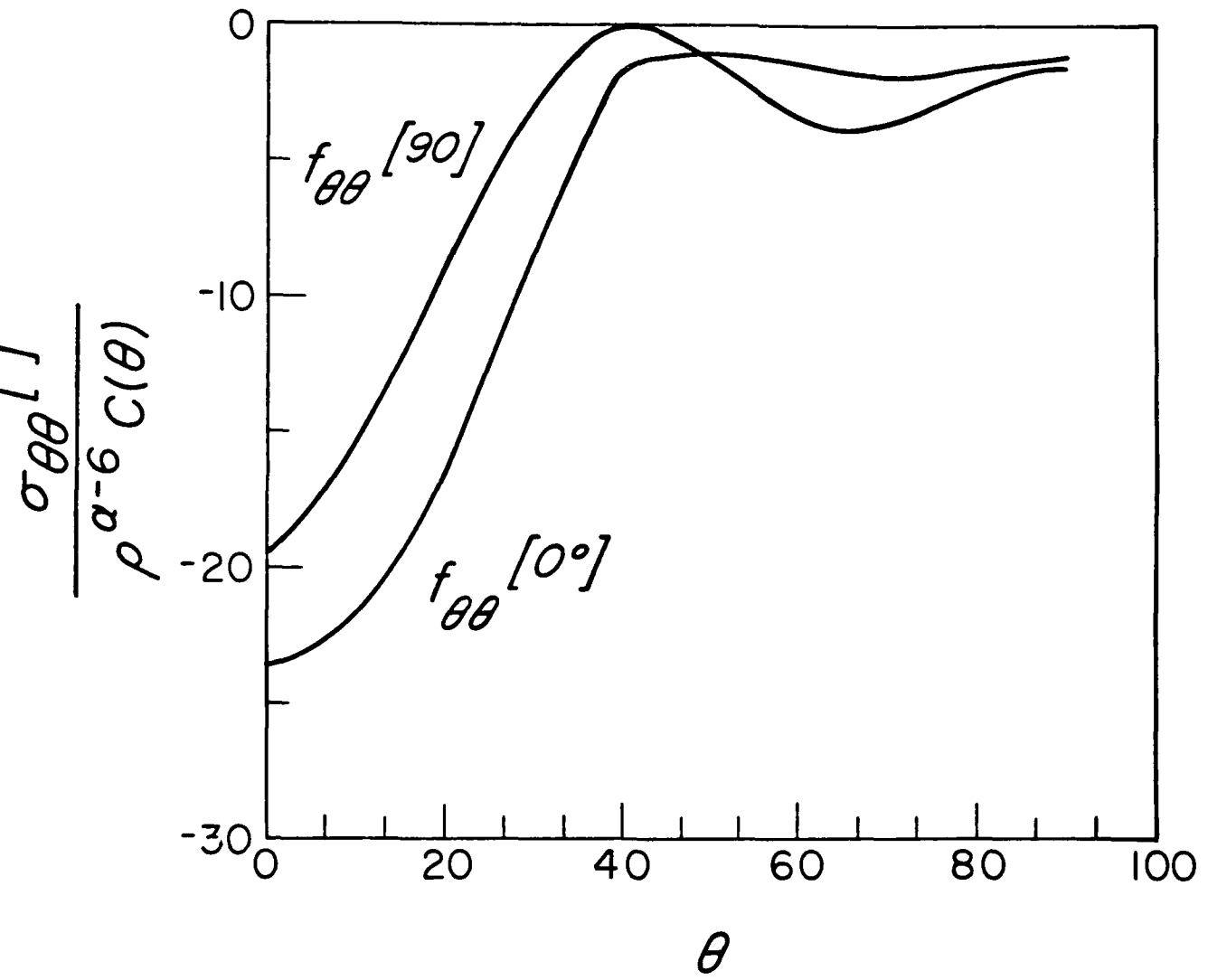

Fig. 10. The stress concentration factor for $\phi = 0^+$ and 0^-.

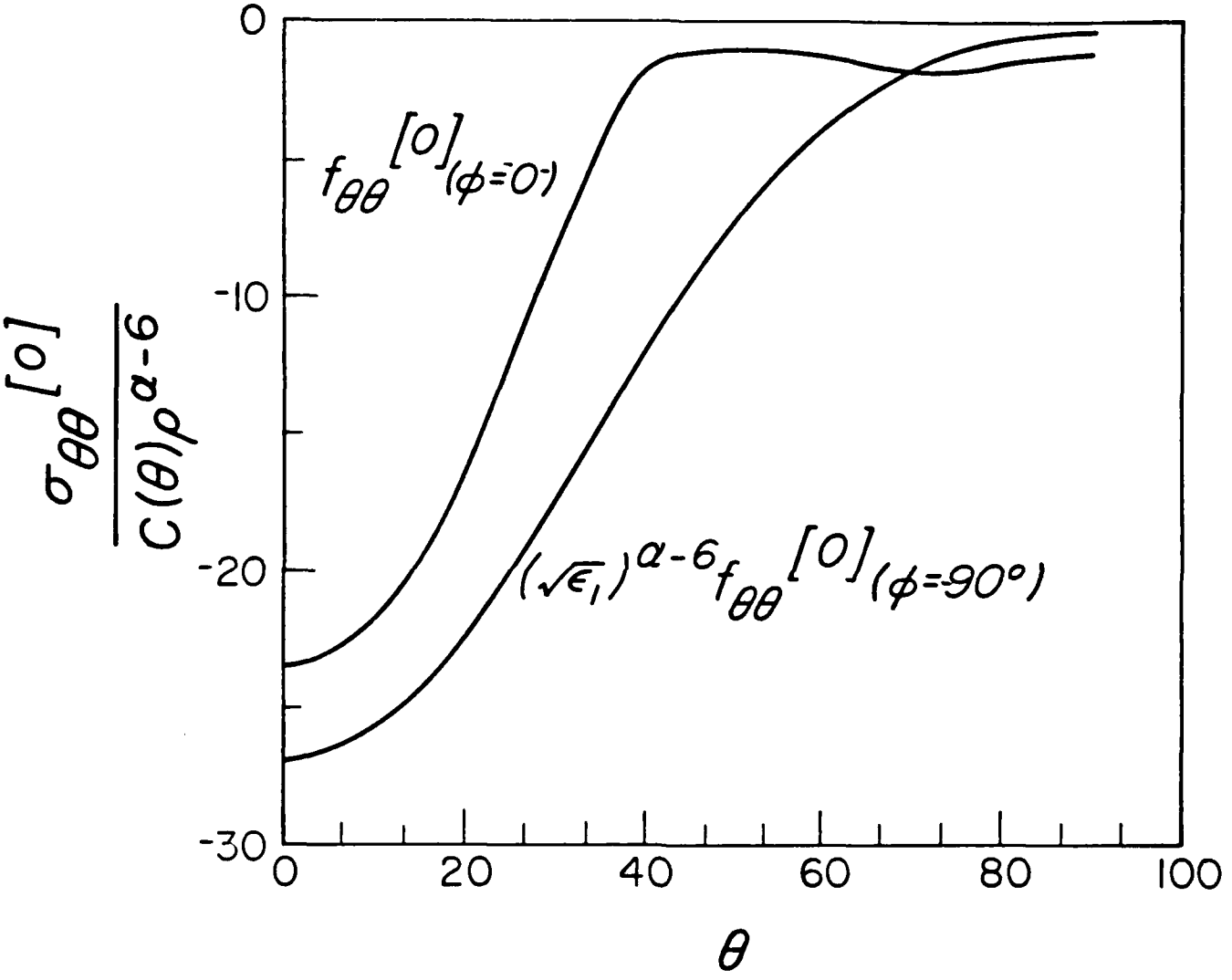

Fig. 11. The stress $\sigma_{\theta\theta}^{[0]}$ for $\phi = 0$ and $\phi = 90^\circ$.

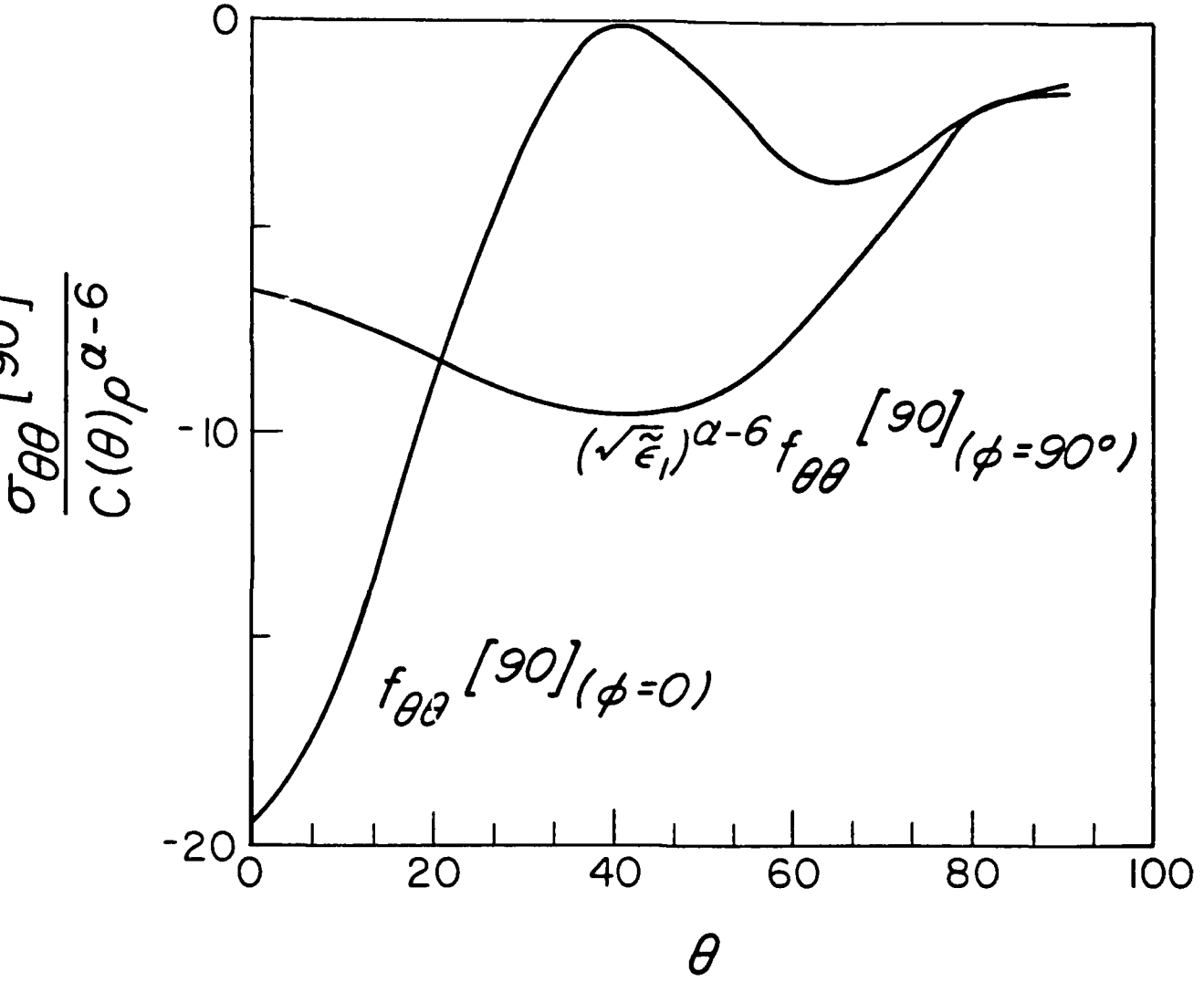

Fig. 12. The stress $\sigma_{\theta\theta}^{[90]}$ for $\phi = 0^{+}$ and $\phi = +90^{\circ}$.

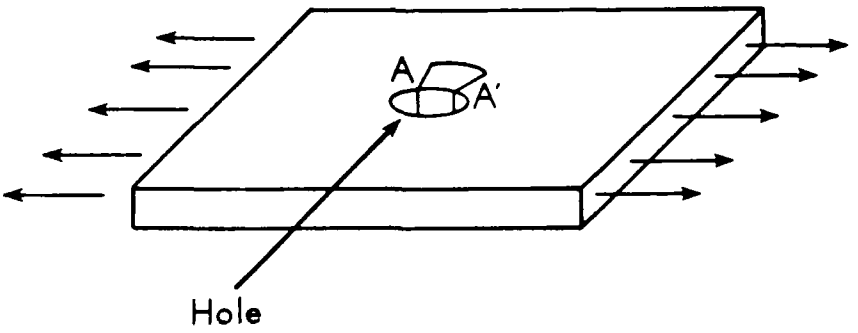

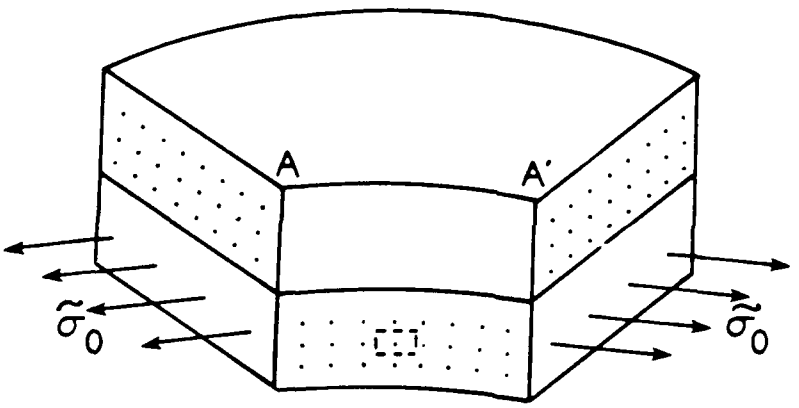

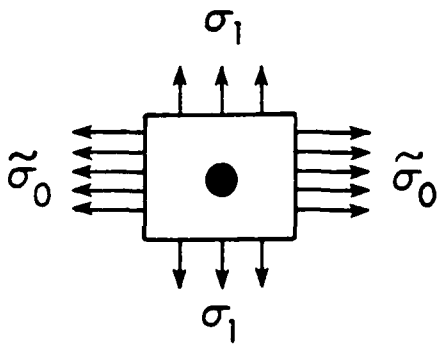

Fig. 13. (a) Geometrical representation.

MICROMECHANICAL CONSIDERATIONS

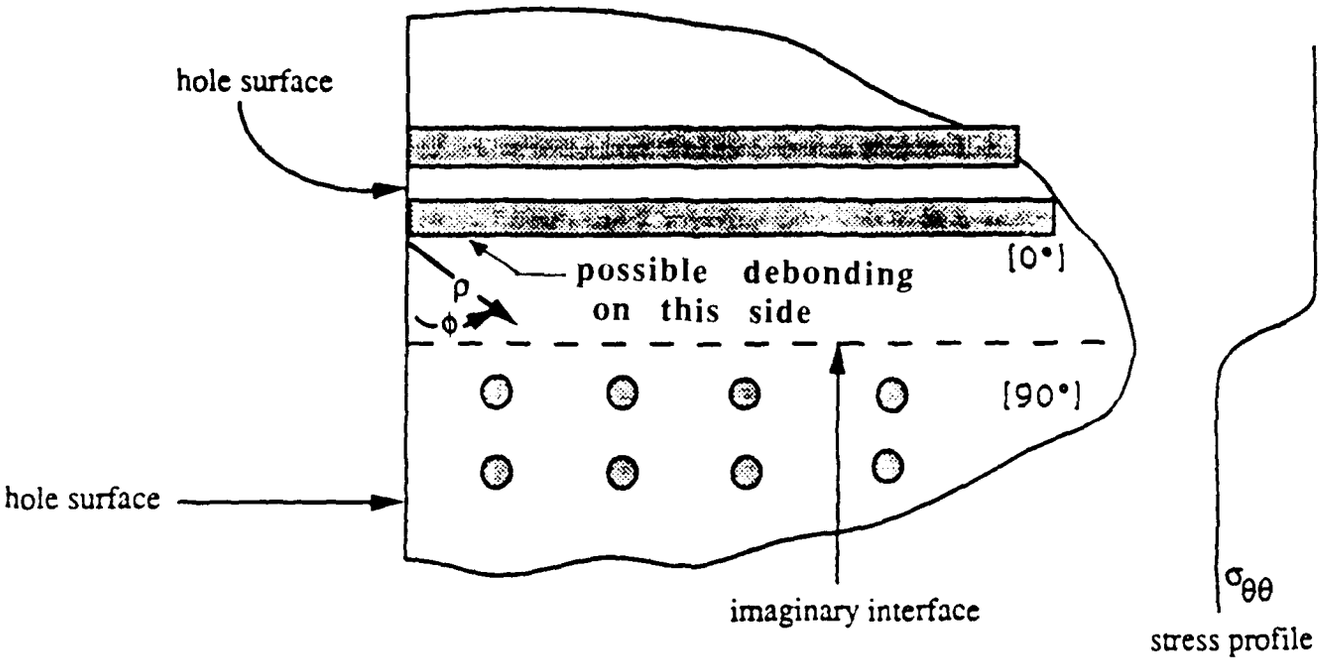

Fig. 13 (b) Local geometry based on micromechanical considerations. (Position $\theta = 90°$)

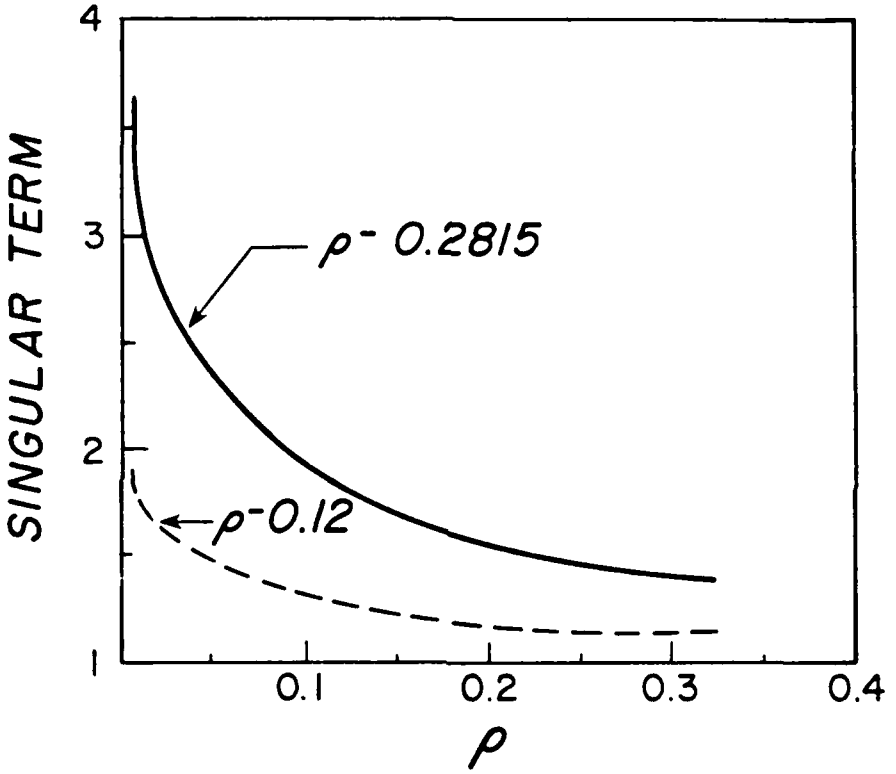

Fig. 14. Comparison of stress singularities.

Part II

ON THE PREDICTION OF FAILURE AT A FIBER/MATRIX INTERFACE IN A COMPOSITE SUBJECTED TO A TRANSVERSE TENSILE LOAD

ABSTRACT

This paper deals with the 3D stress field of a cylindrical fiber which is embedded into a resin matrix. The composite is then subjected to a uniform tensile load σ_0. The strain energy release rate is computed and the criterion is used to predict debonding initiation at the fiber/matrix interface. The analysis shows that this failure is most likely to occur at the free surface, ie the region where the fiber intersects a free surface for example a hole, an edge, or a crack. Moreover, it will occur at approximately (1/10) the load value required for the same failure to commense at the center of the fiber length.

The results are also extended to include a doubly periodic array of fibers which are embedded into a matrix. Based on 3D considerations, the stiffness matrix is shown to increase as the volume fraction of the fibers increases. Similarly, the stress σ_{rr} in the matrix is shown to decrease as the volume fraction of the fibers increases.

INTRODUCTION

It is well recognized that fiber composite materials are very attractive for use in aerospace, automotive and other applications. These composites consist of relatively stiff fibers which are embedded into a lower stiffness matrix. Although in most designs the fibers are aligned so that they are parallel to the direction of the external loads, it is almost impossible to avoid induced transverse stresses which may lead to premature failure of the laminate. An excellent example of this is the case of a filament wound pressure vessel in which the presence of a curvature induces bending as well as transverse stresses (Folias, 1965). However, in order to be able to predict their failing characteristics, particularly in the neighborhood of free surfaces such as holes, edges etc., it is necessary to know the local stress behavior from a 3D point of view.

An overall summary of some of the results, which are based on 2D elasticity considerations can be found in the books by Hull (1981) and by Chamis (1975). In their pioneering work, Adams and Doner (1967) used finite differences to solve the problem of a doubly periodic array of elastic fibers contained in an elastic matrix and subjected to a transverse load. Their results reveal the dependence of the maximum principal stress versus the constituent stiffness ratio (E_f/E_m) for various fiber volume ratios. A few years later, Yu and Sendeckyj (1974) used a complex variable approach to solve the problem of multiple inclusions embedded into an infinite matrix. Their results were subsequently specialized to cases of two and three inclusions thus providing us with futher insight into the strength of the composite. On the other hand, the separation of a smooth circular inclusion from a matrix was investigated by Keer, Dundurs and Kiattikomol (1973). By using finite integral transforms, they were able to reduce the problem to that of a Fredholm integral equation with a weakly singular kernel. Thus, extracting the singular part of the solution, they were able to reduce the remaining problem to a simpler one which lends itself to an effective numerical solution. Their results are very general and are applicable to various combinations of material properties and loads.

In this paper, use of the local, 3D, stress field will be made in order to examine the dependence of the stress σ_{rr}, in the matrix, on the ratio (Gf/Gm). The strain energy release rate will then be computed in order to predict crack initiation at the fiber/matrix interface. Particular emphasis will be placed in the region where fibers meet a free surface as well as at the center of a fiber's length.

FORMULATION OF THE PROBLEM

Let us consider a cylindrical fiber of homogeneous and isotropic material, e.g. a glass fiber, which is embedded into a matrix of also homogeneous and isotropic material.

Futhermore, we assume the matrix to be a rectangular plate with finite dimensions 2w, 2ℓ, and 2h as defined by fig. 1. For simplicity, we assume $\frac{w}{a} > 8$ and $\frac{\ell}{a} > 8$. Such an assumption will guarantee that the boundary planes $x = \pm w$, and $y = \pm \ell$, will not effect the local stress field adjacent to the fiber.* Thus, mathematically, one may consider the boundaries in the x and y directions to extend to infinity. As to loading, the plate is subjected to a uniform tensile load σ_o in the direction of the y-axis and parallel to the bounding planes (see Fig. 1).

In the absence of body forces, the coupled differential equations governing the displacement functions $u_i^{(j)}$ are

$$\frac{1}{1-2\nu_j} \frac{\partial e^{(j)}}{\partial x_i} + \nabla^2 u_i^{(j)} = 0, \; i = 1,2,3, \; j = 1,2, \qquad (1)$$

where ∇^2 is the Laplacian operator, ν_j is Poisson's ratio, $u_i^{(1)}$ and $u_i^{(2)}$ represent the displacement functions in media 1 (matrix) and 2 (fiber) respectively, and

$$e^{(j)} = \frac{\partial u_i^{(j)}}{\partial x_i} \; ; \; i = 1,2,3 \; ; \; j = 1,2. \qquad (2)$$

The stress-displacement relations are given by Hooke's law as

---

* This can be seen from the results which were recently reported by (Penado and Folias (1989).

$$\sigma_{i\ell}^{(j)} = \lambda_j \; e_{kk}^{(j)} \; \delta_{i\ell} + 2G^{(j)} \, e_{i\ell}^{(j)} , \qquad (3)$$

where λ_j and G_j are the Lame' constants describing media 1 and 2.

THE SOLUTION FOR ONE FIBER

A. Region where fiber intersects the free edge

This problem was recently investigated by the author (Folias 1989) who was able to recover, explicitly, the three dimensional stress field adjacent to the surface of the fiber* . Without going into the mathematical details, the displacement and stress fields for the matrix are given in terms of the local coordinate system (see fig. 2) by:

(i) displacement field:

$$u^{(1)} = A_n \rho^{\alpha-1} \sin\theta \{B [2 (1-\nu_1) \cos (\alpha-1)\phi - (\alpha-1) \sin\phi \sin(\alpha-2)\phi] \quad (4)$$
$$- (\alpha+1) [(1-2\nu_1) \sin (\alpha-1)\phi + (\alpha-1) \sin\phi \cos (\alpha-2) \phi]\} \cos(2n\theta)$$

$$v^{(1)} = A_n \rho^{\alpha-1} \cos\theta \{B [2 (1-\nu_1) \cos (\alpha-1)\phi - (\alpha-1) \sin\phi \sin(\alpha-2)\phi] \quad (5)$$
$$- (\alpha+1) [(1-2\nu_1) \sin (\alpha-1) \phi + (\alpha-1) \sin\phi \cos (\alpha-2)\phi] \} \cos(2n\theta)$$

$$w^{(1)} = A_n \rho^{\alpha-1} \{B [- (1-2\nu_1) \sin (\alpha-1)\phi + (\alpha-1) \sin\phi \cos (\alpha-2) \phi] \quad (6)$$
$$- (\alpha+1) [2 (1-\nu_1) \cos (\alpha-1)\phi + (\alpha-1) \sin\phi \sin(\alpha+2) \phi]\} \cos(2n\theta)$$

(ii) stress field:

$$\sigma_{rr}^{(1)} = 2G^{(1)} (\alpha-1) A_n \rho^{\alpha-2} \{B [2 \cos (\alpha-2)\phi - (\alpha-2) \sin\phi \sin(\alpha-3)\phi] \quad (7)$$
$$- (\alpha+1) [\sin (\alpha-2)\phi + (\alpha-2) \sin\phi \cos (\alpha-3)\phi] \} \cos(2n\theta)$$

$$\sigma_{\theta\theta}^{(1)} = 4\nu_1 G^{(1)} (\alpha-1) A_n \rho^{\alpha-2} \{B \cos (\alpha-2)\phi - (\alpha+1) \sin(\alpha-2)\phi\} \cos(2n\theta) \quad (8)$$

---

* A similar analysis for a transversely isotropic fiber meeting a free surface has recently been completed and the results will be reported soon.

$$\sigma_{zz}^{(1)} = 2G^{(1)} (\alpha-1) A_n \rho^{\alpha-2} \left\{ B (\alpha-2) \sin\phi \sin(\alpha-3)\phi \right. \tag{9}$$
$$\left. + (\alpha+1) \left[(\alpha-2) \sin\phi \cos(\alpha-3)\phi - \sin(\alpha-2)\phi \right] \right\} \cos(2n\theta)$$

$$\tau_{rz}^{(1)} = 2G^{(1)} (\alpha-1) A_n \rho^{\alpha-2} \left\{ B \left[\sin(\alpha-2)\phi + (\alpha-2) \sin\phi \cos(\alpha-3)\phi \right] \right. \tag{10}$$
$$\left. - (\alpha+1) (\alpha-2) \sin\phi \sin(\alpha-3)\phi \right\} \cos(2n\theta)$$

$$\tau_{r\theta}^{(1)} = \tau_{\theta z}^{(1)} = 0, \tag{11)-(12}$$

where n = 0,1,2,... and B is a function of the material constants and A_n is a constant to be determined from the boundary conditions far away from the fiber*. In general, the characteristic value of α depends on the material constants of the fiber as well as of the matrix. A typical example is given in fig. 3.

Upon examination of the stress field, the following remarks are worthy of note. First, the stress field in the neighborhood where the fiber meets the free surface is signular. Moreover, in the limiting case of a perfectly rigid inclusion this singularity strength reaches the value of 0.2888. Second, boundary conditions $\sigma_{zz}^{(1)}$, $\tau_{xz}^{(1)}$ and $\tau_{yz}^{(1)}$ are satisfied as a consequence of the odd functional behavior in ϕ, which points to the presence of a boundary layer solution as one approaches the free surface. Third, on the free surface the radial stress is $(1/\nu_1)$ times the circumpherential stress. This suggests, therefore, that if a crack was to initiate, it would propagate along, (or very very close to) the fiber/matrix interface. Clearly, the occurance of either adhesive or cohesive failure will depend on the relative strengths of the interface, of the fiber, and of the matrix. All things being equal, the analysis shows the stresses to be highest at the interface, thus pointing to an adhesive type of failure.

* for one fiber n=0,1., while for a periodic extension n=0,1,2,..

B. Interior region

The, 3D, stress field for this region has also been recovered by Penado and Folias (1989) and the results for various (a/h) and (G_2/G_1) ratios may be found in the literature. The results have subsequently been extended (Folias and Liu, 1990) to also include a layer of modified matrix around the fiber. Thus for $\nu_1 = 0.34$, $\nu_2 = 0.22$ and $(G_2/G_1) = 16.67$ the stresses $\sigma_{rr}^{(1)}$ and $\sigma_{\theta\theta}^{(1)}$ at r = a and for all $|z| \leq h$ are given in figs 4 and 5 respectively. Finally, fig. 6 (for λ=0) shows the variation of the stress $\sigma_{rr}^{(1)}$ as a function of the ratio (G_2/G_1).

INTERFACE FAILURE CLOSE TO THE FREE SURFACE

A closer inspection of the local stress field shows that a crack is most likely to initiate at the location $\theta = 0$ and subsequently propagate along the fiber/matrix interface until it reaches a nominal value of the arc length beyond which it will advance into the matrix. Moreover, once the crack begins to propagate, it will simultaneously propagate along the interface and parallel to the axis of the fiber (mode III). Thus, crack propagation will be governed initially by a mode I failure and subsequently by a combination of mode I and mode III failure. It is now possible for us to examine the first stage of the failing process and to obtain an estimate of the debonded arc length as well as an estimate of the critical transverse stress for crack initiation.

As a practical matter, we will consider the special case of a glass fiber embedded into an epoxy matrix with the following properties

$$G_1 = 2.10\,\text{GPa} \qquad \nu_1 = 0.34 \qquad (13)$$
$$G_2 = 35.00\,\text{GPa} \qquad \nu_2 = 0.22\,.$$

Without going into the numerical details, the constants α, A and B for this example are found to be* :

* The constant A has been determined by comparing the displacement $w^{(1)}$, as well as the stress $\sigma_{rr}^{(1)}$ at $\theta = 0$, at z = h and for (a/h) = 0.5 with the work of Penado and Folias (1989).

$A \equiv \sum_n A_n$.

$$\alpha = 1.7511,\ G^{(1)}\, A\, a^{\alpha-2} \approx 0.6349\, \sigma_o\,,\quad B \approx 2.1302\,, \tag{14}$$

where σ_o now has the units of GPa. Thus, from equations (7)-(12) one has

(i) at $\phi = 0$ and $\theta = 0$:

$$\sigma_{rr}^{(1)} \approx 4.0633\, \sigma_o \left(\frac{r-a}{a}\right)^{-0.2489} \tag{15}$$

$$\sigma_{\theta\theta}^{(1)} = \nu_1\ \sigma_{rr}^{(1)}, \tag{16}$$

(ii) at $\phi = \pi/2$ and $\theta = 0$:

$$\sigma_{rr}^{(1)} \approx 1.9163\, \sigma_o \left(\frac{h-z}{h}\right)^{-0.2489} \tag{17}$$

$$\sigma_{\theta\theta}^{(1)} \approx 0.4844\ \sigma_{rr}^{(1)} \tag{18}$$

$$\tau_{rz}^{(1)} \approx -\,0.2930\, \sigma_{rr}^{(1)}. \tag{19}$$

It is clear now from equations (15) and (16) that crack failure is most likely to initiate and subsequently propagate along the fiber/matrix interface rather than perpendicular to it. Similarly, equations (17) and (19) suggest that failure in the direction parallel to the axis of the fiber is dominated first by a mode I and second by a mode III type of failure. It may also be noted that $\sigma_{rr}^{(1)}$ attains a maximum at $\theta = 0$ and descreases as one travels along the surface of the fiber.

Finally, based on 3D considerations, the stress field away from the edges, $z = \pm h$, and in the interior of the plate was shown to be non-singular (Penado and Folias 1989, Folias and Liu 1990) with*

$$\sigma_{\theta\theta}^{(1)} = 0.4090\ \sigma_{rr}^{(1)} = 0.4090\,(1.4281\, \sigma_o) = 0.5841\, \sigma_o\,, \text{ at } \theta = 0 \tag{20a}$$

---

* These results are valid for a ratio of (a/h) = 0.05 and subject to the assumption that $(\frac{w}{a}) > 8$ and $(\ell/a) > 8$ in which case the end boundaries in x and y have insignificant effects on the local to the fiber stress field.

at r = a and z = 0. Comparing this value with that of the corresponding plane strain solution

$$\sigma_{\theta\theta}^{(1)} = \frac{\nu_1}{1-\nu_1}\ \sigma_{rr}^{(1)} = 0.5152\ \sigma_o\,, \quad \text{at } \theta = 0 \tag{20b}$$

one notices that it is approximately 13% higher in value due to the presence of the stresses in the third dimension.

It is now possible for us to obtain an approximate criterion for debonding along the fiber/matrix interface based on Griffith's theory of fracture. Thus, following the work of Toya (1974), if one assumes the presence of an interface crack of length $2a\beta$ and if futhermore takes into account the local 3D stress field, then Toya's result may be written as

$$(1/16)\,(1.1337\sigma_o)^2\, k\, a\, \tilde{A}_1\, (1+4\,\varepsilon^2)\, \pi\, N_o\, \bar{N}_o \sin\beta \exp\left[2\,\varepsilon\,(\pi-\beta)\right] = 2\gamma_{12} \tag{21}$$

where

$$k = \frac{1+k_2}{1+k_2 + (1+k_1)\ (G_2/G_1)} \tag{22}$$

$$k_i = \begin{cases} 3-4\nu_i & \text{for plane strain} \\ \dfrac{3-\nu_i}{1+\nu_i} & \text{for plane stress} \end{cases} \tag{23}$$

$$\tilde{A}_1 = \frac{k}{4\,G_1}\left\{1 + k_1 + (1+k_2)\,(G_1/G_2)\right\} \tag{24}$$

$$\varepsilon = -\frac{1}{2\pi}\,\ell n\left[\frac{1+k_2\,(G_1/G_2)}{k_1 + (G_1/G_2)}\right] \tag{25}$$

$$N_o = G_o - \frac{1}{k} - \frac{2\,(1-k)}{k}\ \frac{1+k_2\,(G_1/G_2)}{k_1 + (G_1/G_2)}\ \exp\left[\beta\,(2\varepsilon - i)\right] \tag{26}$$

$$G_o = \frac{1-(\cos\beta + 2\varepsilon\sin\beta)\exp\left[2\varepsilon\,(\pi-\beta)\right] + (1-k)\,(1+4\varepsilon^2)\sin^2\beta}{2-k-k\,(\cos\beta + 2\varepsilon\sin\beta)\exp\left[2\varepsilon\,(\pi-\beta)\right]}\,, \tag{27}$$

where $\bar{N}_o$ is the complex conjugate of N_o, γ_{12} is the specific surface energy of the interface and β the angle of debonded interface (see Fig. 7) while it is true that this type of approach does not provide results for the exact initiation of an interface crack problem, ie from a condition of perfectly bonded interface to that of a partially debonded interface, it does, however, provide a very good first approximation to this complex phenomenon. The author is well aware of that and is presently continuing his work along such lines and with some promise.

Upon rearranging, equation (21) can be written in the form*

$$\frac{2\gamma_{12}}{\sigma_o^2 a} = (1.2853)\, F\,(\nu_i, G_i; \beta), \tag{28}$$

where F is a function of the material constants and the angle β of the debonded interface. A plot of this equation for conditions of plane stress, as well as of plane strain, is given in Fig. 8. In both cases the maximum occurs at $\beta = 60°$. Beyond this angle, the crack will gradually curve away from the interface and into the matrix.

In order for us to obtain an estimate for the critical stress for crack initiation we let $\beta \to 0^+$, ie very small but not zero. Thus, for our example

$$(\sigma_o)_{cr}\ \sqrt{2\,a\,\beta} \approx 1.8186\,\sqrt{\gamma_{12}\,G_1};\quad \text{at } z = 0. \tag{29a}$$

On the other hand, in the neighborhood of the free surface, the applied stress is much higher because of the singularity presence. In order to overcome this difficulty, one may average the local stress over a distance equal to 10% of that of the radius, ie.

* It should be noted that at the crack ends the stress field oscillates and that some overlap of the crack faces takes place. This matter is well recognized and has been documented by Williams (1952), Rice et al. (1965) and England (1965). The region where this occurs, however, is so small (less than a x 10^{-3}) that eq. (28) provides a good approximation.

$$(\sigma_o)_{eff} = \frac{1}{(0.1a)} \int_0^{0.1a} (4.0633\,\sigma_o) \left(\frac{\xi}{a}\right)^{-0.2489} d\xi \qquad (30)$$

$$\approx 9.5958\,\sigma_o\,.$$

Thus*

$$(9.5958\,\sigma_o)_{cr} \sqrt{2\,a\,\beta} \approx 1.8146 \sqrt{\gamma_{12}\,G_1}\,; \quad \text{at } z \approx \pm h. \qquad (29b)$$

Combining next eqs. (29a) and (29b) one finds

$$\frac{(\sigma_o)_{cr}\,|_{at\ z=h}}{(\sigma_o)_{cr}\,|_{at\ z=0}} \approx 0.10, \qquad (31)$$

ie. the critical loading stress which may cause failure close to a free surface is approximately (1/10) of the critical stress required to cause the same failure at the center of the fiber's length. Thus, all things being equal, a crack will initiate at the free surface and will propagate along the periphery of the fiber/matrix interface as well as parallel to the axis of the fiber.

Focusing next our attention on the advancement of the crack along the periphery of the fiber we conclude that the crack will advance itself to a cricital angle of $\beta \approx 60°$. Once the crack has reached* $\theta = 60°$, the local geometry is similar to that of a hole. This problem has also been investigated for the, 3D, stress field close to a free surface (Folias, 1987), as well as in the interior of the plate (Folias and Wang 1986). Without going into the details, at z=h, it was found that

$$\frac{\sigma^{(1)}_{\theta\theta}}{\sigma^{(1)}_{rr}} = -(1+\nu_1) = -1.34, \qquad (32)$$

suggesting, therefore, that the failure now is governed by the stress $\sigma^{(1)}_{\theta\theta}$ which attains its maximum value at $\theta = \pi/2$. Thus, the crack will begin to curve into

* The reader may notice that the right hand side of equation (29b) differs from (29a) because it is based on plane stress.

the matrix until its direction becomes perpendicular to that of the applied load.

PERIODIC ARRAY OF FIBERS

The previous results were based on the presence of one fiber only. It is now desirable to extend these results to also include a doubly periodic array of fibers which are embedded into a matrix. For this reason, we assume, a periodic arrangement of the type shown in fig. 9. Following the same method of solution as that of Penado and Folias (1989), one finds* at z=0 the stresses $\sigma_{rr}^{(1)}$ and $\sigma_{\theta\theta}^{(1)}$, for $\nu_1 = 0.34$, $\nu_2 = 0.22$ and various (G_2/G_1) ratios, shown in figs. 6 and 10. Two observations are worthy of note. First, beyond a certain ratio of (G_2/G_1) the stress $\sigma_{rr}^{(1)}$ reaches an asymptotic value. Such trend was also found by Adams (1967) based on 2D considerations. Second, as the volume of fibers increases the stress $\sigma_{rr}^{(1)}$ decreases by as much as 40% (see fig. 11). Finally, in fig. 12 we plot the stiffness ratio versus the fiber volume fraction V_f.

Returning next to the strain energy release rate, equation (21) is still a good approximation provided that σ_o is replaced by the following effective load stress

$$(\sigma_o)_{\text{effective periodic}} \approx \left\{ \frac{\sigma_{rr}^{(1)}|_{\lambda}}{\sigma_{rr}^{(1)}|_{\lambda=0}} \right\} \sigma_o \; ; \text{ for } z = 0. \tag{33}$$

Unfortunately, in order to obtain a similar expression for z=h, one needs to establish whether the order of the singularity strength increases as adjacent

---

* The results are valid for all fibers which are at least four diameters away from the bounding planes $x = \pm w$ and $y = \pm \ell$. The solution and the details are similar to those discussed by Penado and Folias (1989) except that one now has $\cos(2n\theta)$, n= 0,1,2,..., where the remaining unknown coefficients are determined from the boundary conditions of the geometrical cell configuration. The present results, are based on n = 0,..., N = 20 terms which provide accurate results in the region $|z/h| < 1/2$. However, many more terms are needed in order to obtain accurate results particularly in the neighborhood of $z = \pm h$. We are presently working on this and the results for this problem, as well as for the problem of stresses due to temperature missmatch, will be reported in the near future.

fibers approach the fiber in question. In view of some previous work the author conjectures that this may very well be the case. Thus, the following fundamental questions come to mind. How close must adjacent fibers be before the order of the singularity strength is affected? Does a certain separation distance or a certain periodic array of fibers exists which leads to an optimal state of stress? Based on 3D considerations, Penado and Folias (1989) have shown that when fibers are placed four fiber diameters apart, center to center, practically all fiber interactions have subsided, including those at the free surface z=h. The author suspects, however, that when fibers are placed two diameters apart, center to center, the singularity strength will be affected. Naturally, this is a conjecture that needs to be investigated.

CONCLUSIONS

Based on a 3D analytical solution, we have shown that fiber/matrix debonding is most likely to occur close to a free surface. Thus, regions where fibers intersect free surfaces, eg. holes, cut outs, edges, cracks etc. are potential trouble spots. Moreover, the strain energy release rate (eq. 28) may be used to predict crack initiation in the center of the fiber length (eq. 29a), as well as at the free surface (eq. 29b). Moreover, fiber/matrix debonding at a free surface will occur at approximately (1/10) the load value required for the same type of failure to occur at the center of the fiber length. Such information on crack initiation is particularly important for the proper understanding of damage evolution.

Alternatively, the strain energy release rate for a periodic array of fibers of the type shown in fig. 9 may, at z=0, be approximated by eq. (28) in conjunction with eq. (33). A similar expression applicable to the neighborhood of the free surface requires that one must first establish whether the strength of the singularity is indeed affected as the fiber volume increases. For $\bar{V}_f \leq 0.05$, however, it has been shown* that no such interaction effects are present.

As a final remark, we note that if the bond at the interface does not fail the analysis shows that there exists a stress magnification factor in the resin which attains a maximum between the fibers. This maximum stress

* See Panado and Folias (1989).

magnification occurs along the line $\theta = 0°$ and at a distance $r = 1.2a$ from the center of the fiber** .

ACKNOWLEDGEMENT

This work was supported in part by the Air Force Office of Scientific Research Grant No. AFOSR-87-0204. The author wishes to thank Lt. Col. G. Haritos for this support and for various discussions.

REFERENCES

Adams, D.F. and Doner, D.R., 1967, "Transverse Normal Loading of a Unidirectional Composite", J. of Composite Materials, Vol. 1, pp. 152-164.

Chamis, C.C., 1975, Edited, "Composite Materials", Academic Press, Vol. 1-8.

England, A.H., 1965, "A Crack Between Dissimilar Media", Journal of Applied Mechanics pp. 400-402.

Folias, E.S., 1989, "The 3D Stress Singularities at the Intersection of a Cylindrical Inclusion and a Free Surface", International Journal of Fracture, Vol. 39, pp. 25-34.

Folias, E.S., 1987, "The 3D Stress Field at the Intersection of a Hole and a Free Surface", International Journal of Fracture, Vol. 35, No. 3, pp. 187-194.

Folias, E.S., 1965, "An Axial Crack in a Pressurized Cylindrical Shell", International Journal of Fracture, Vol. 1, pp. 20-46.

Folias, E.S. and Liu, J., 1990, "The 3D Stress Field of a Cylindrical Fiber Embedded into a Matrix with a Layer of Modified Matrix Around the Fiber" in preparation.

Folias, E.S. and Wang, J.J., 1986, "On the Three-Dimensional Stress Field Around a Circular Hole in a Plate of an Arbitrary Thickness", University of Utah Technical Report.

Hull, D., 1981, "An Introduction to Composite Materials", Cambridge University Press.

Keer, L.M., Dundurs, J., Kiattikomol, k., 1973, "Separation of a Smooth Cricular Inclusion from a Matrix", Int. Journal of Engineering Science, Vol. 11, pp. 1221-1233.

** This condition is valid for all $0 \leq z < h$.

Penado, F.E., Folias, E.S., 1989, "The Three-Dimensional Stress Field Around a Cylindrical Inclusion in a Plate of Arbitrary Thickness", International Journal of Fracture, Vol. 39, pp. 129-146.

Rice, J.R. and Sih, G.C., 1965, Journal of Applied Mechanics, Transaction ASME, Series E 32, p. 418.

Toya, M., 1974, "A Crack Along the Interface of a Circular Inclusion Embedded in an Infinite Solid", Journal of Mechanics and Physics of Solids, Vol. 22, pp. 325-348.

Williams, M.L., 1952, Journal of Applied Mechanics, Transactions ASME, 19, p. 526.

Yu, I.W. and Sendeckyj, G.P., 1974, "Multiple Circular Inclusion Problems in Plane Elastostatics," pp. 215-220.

FIGURE CAPTIONS

Fig. 1. Geometrical and loading configuration.

Fig. 2. Definition of local coordinates.

Fig. 3. Singularity strength for isotropic fiber and isotropic matrix versus G_2/G_1.

Fig. 4. Stress $\sigma_{rr}^{(1)}$ at r=a, θ=0 and for $\nu_1 = 0.34$, $\nu_2 = 0.22$ and $(G_2/G_1) = 16.67$, accross the thickness.

Fig. 5 Stress $\sigma_{\theta\theta}^{(1)}$ at r=a, θ=0 and for $\nu_1 = 0.34$, $\nu_2 = 0.22$ and $(G_2/G_1) = 16.67$, across the thickness.

Fig. 6 Stress $\sigma_{rr}^{(1)}$ at r=a, θ=0 and for $\nu_1 = 0.34$, $\nu_2 = 0.22$, versus the ratio (G_2/G_1).

Fig. 7 Fiber/matrix interface crack under transverse loading.

Fig. 8 Strain energy release rate for plane stress and plane strain conditions for $\nu_1 = 0.34$, $\nu_2 = 0.22$ and $(G_2/G_1) = 16.67$.

Fig. 9 Periodic array of fibers of length 2h, embedded into a matrix.

Fig. 10 Stress $\sigma_{rr}^{(1)}$ at r=a, θ=0 and for $\nu_1 = 0.34$, $\nu_2 = 0.22$, versus the ratio (G_2/G_1).

Fig. 11 Stress $\sigma_{\theta\theta}^{(1)}$ at r=a, versus V_f, for $(G_2/G_1) = 16.67$ $\nu_1 = 0.34$, $\nu_2 = 0.22$.

Fig. 12. Stiffness ratio versus V_f for $(G_2/G_1) = 16.67$, $\nu_1 = 0.34$ and $\nu_2 = 0.22$.

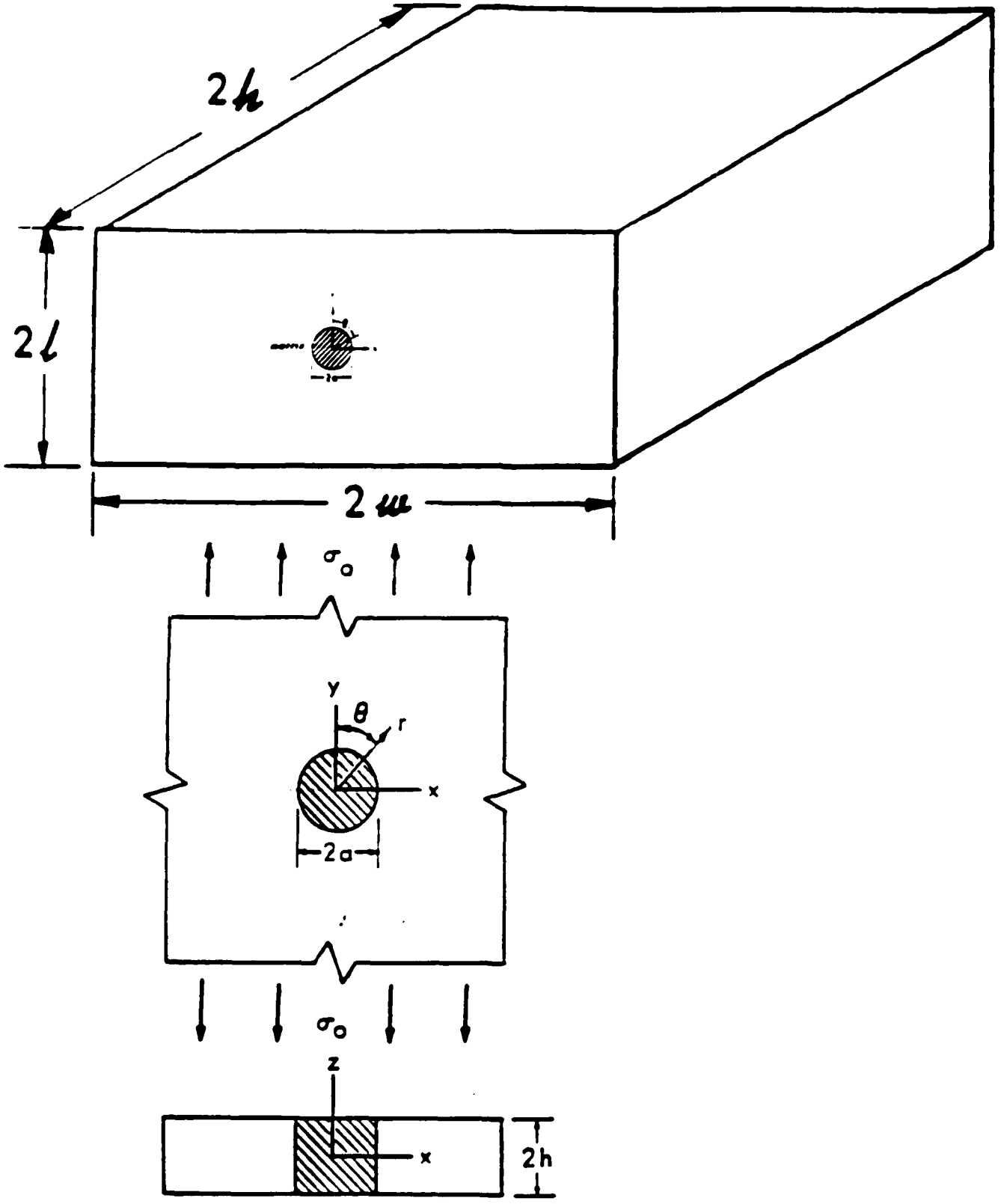

Fig. 1. Geometrical and loading configuration.

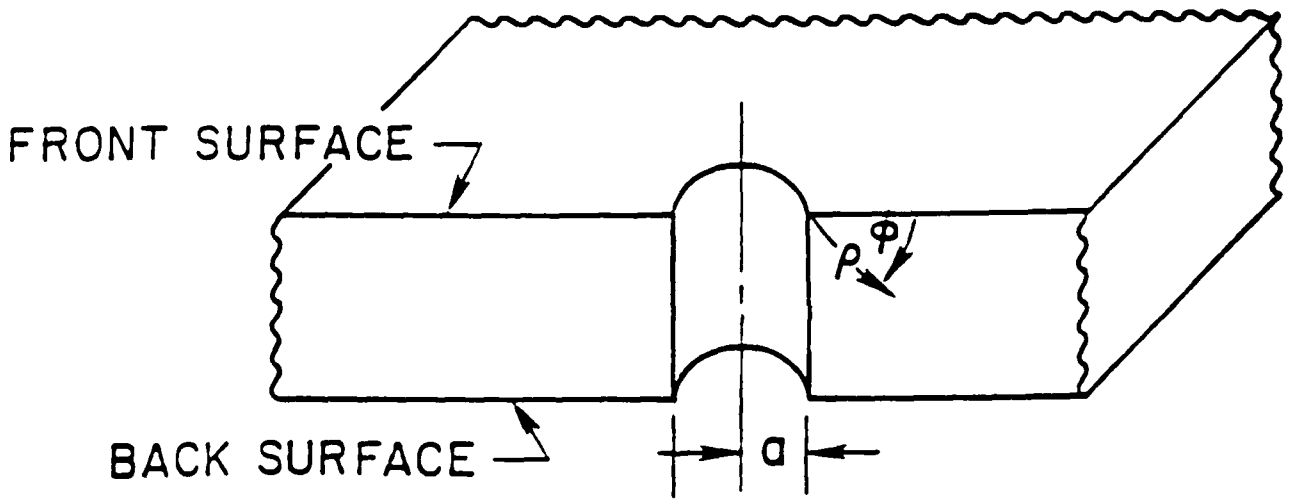

Fig. 2. Definition of local coordinates.

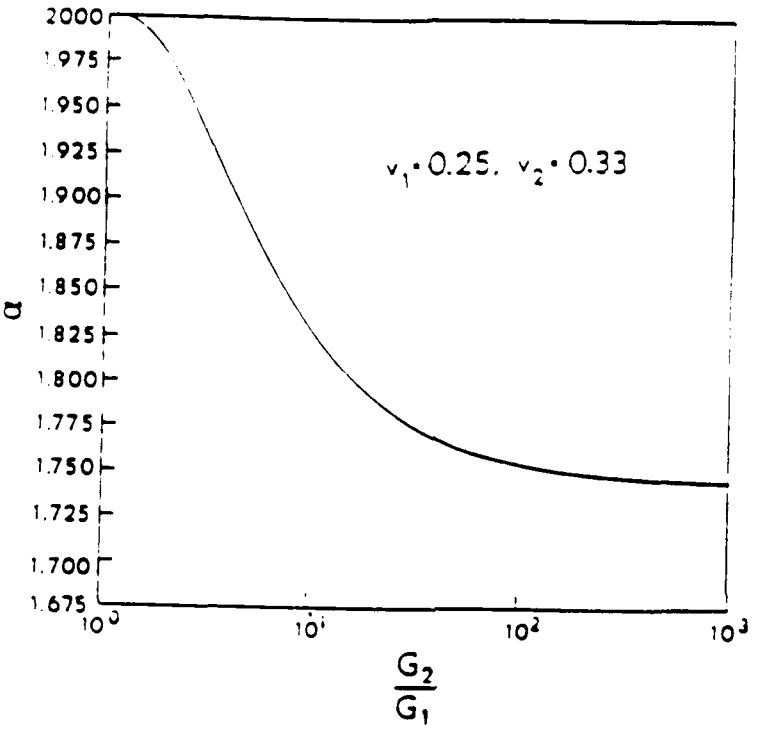

Fig. 3. **Singularity strength for isotropic fiber and isotropic matrix versus G_2/G_1.**

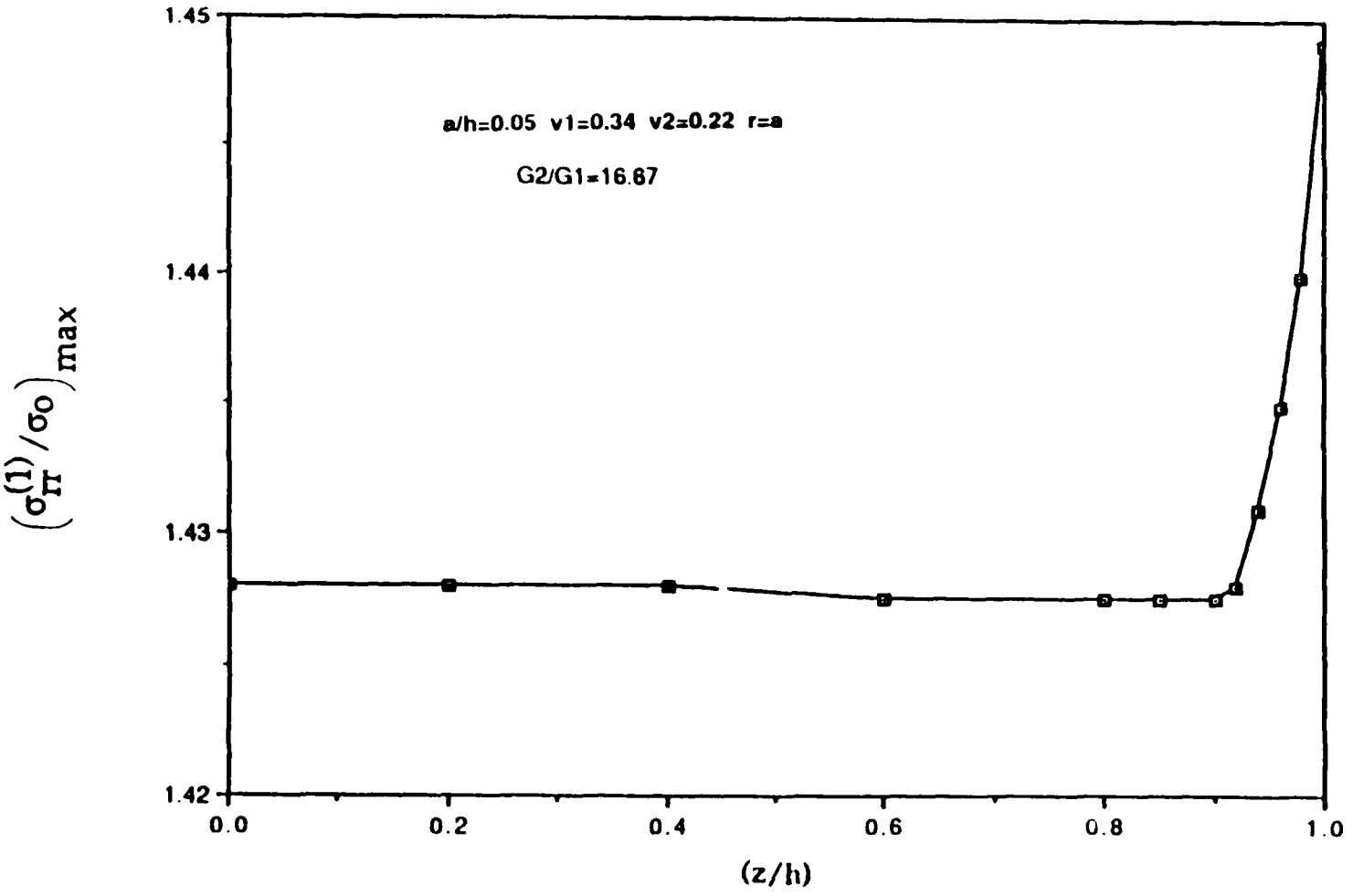

Fig. 4. Stress $\sigma_{rr}^{(1)}$ at r=a, θ=0 and for $\nu_1 = 0.34$, $\nu_2 = 0.22$ and $(G_2/G_1) = 16.67$, accross the thickness.

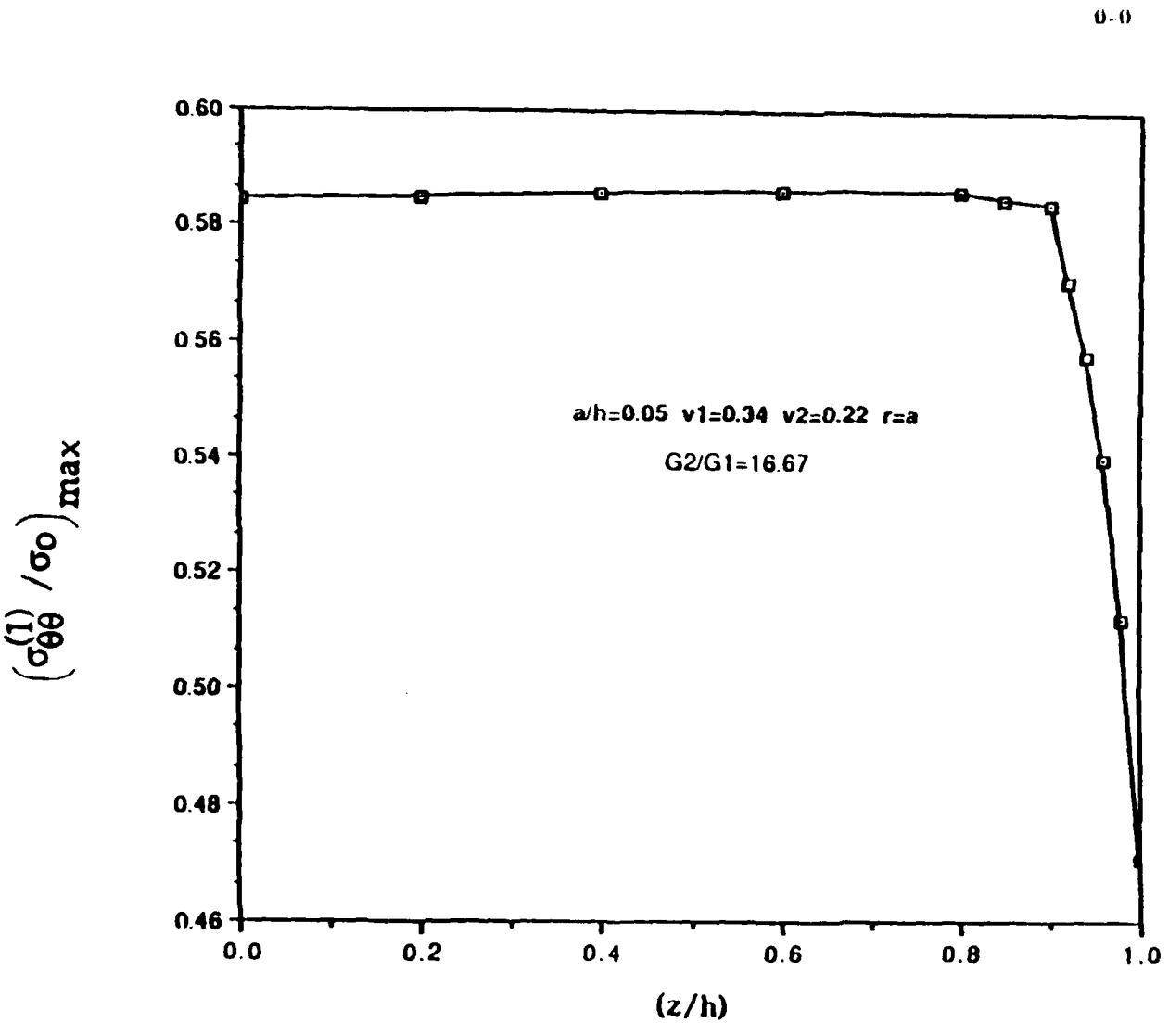

Fig. 5 Stress $\sigma^{(1)}_{\theta\theta}$ at r=a, θ=0 and for $\nu_1 = 0.34$, $\nu_2 = 0.22$ and $(G_2/G_1) = 16.67$, across the thickness.

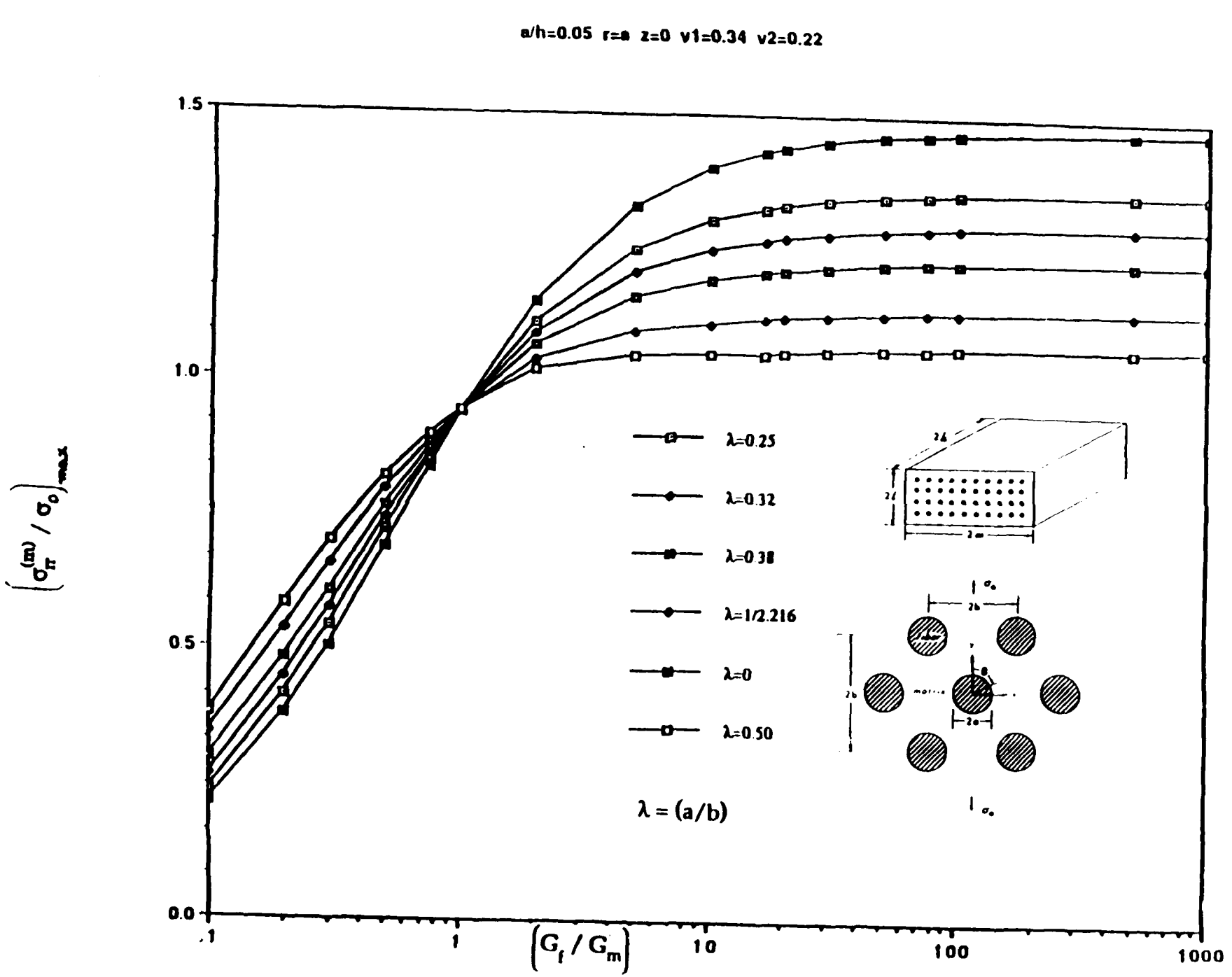

Fig. 6. max stress σ_{rr} at the center of a fiber for a fiber diameter to fiber length ratio of 0.05 versus Gf/Gm.

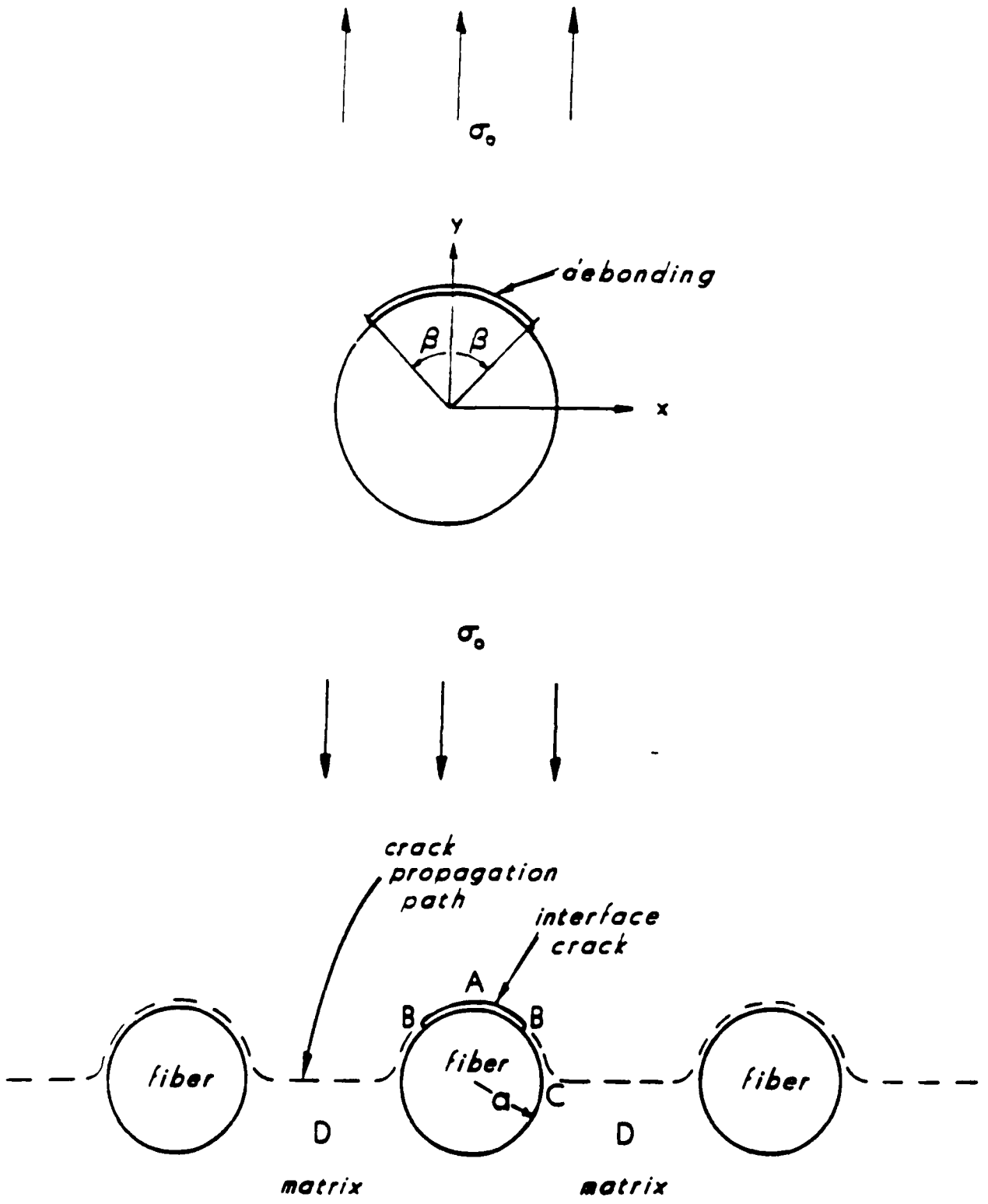

Fig. 7 Fiber/matrix interface crack under transverse loading.

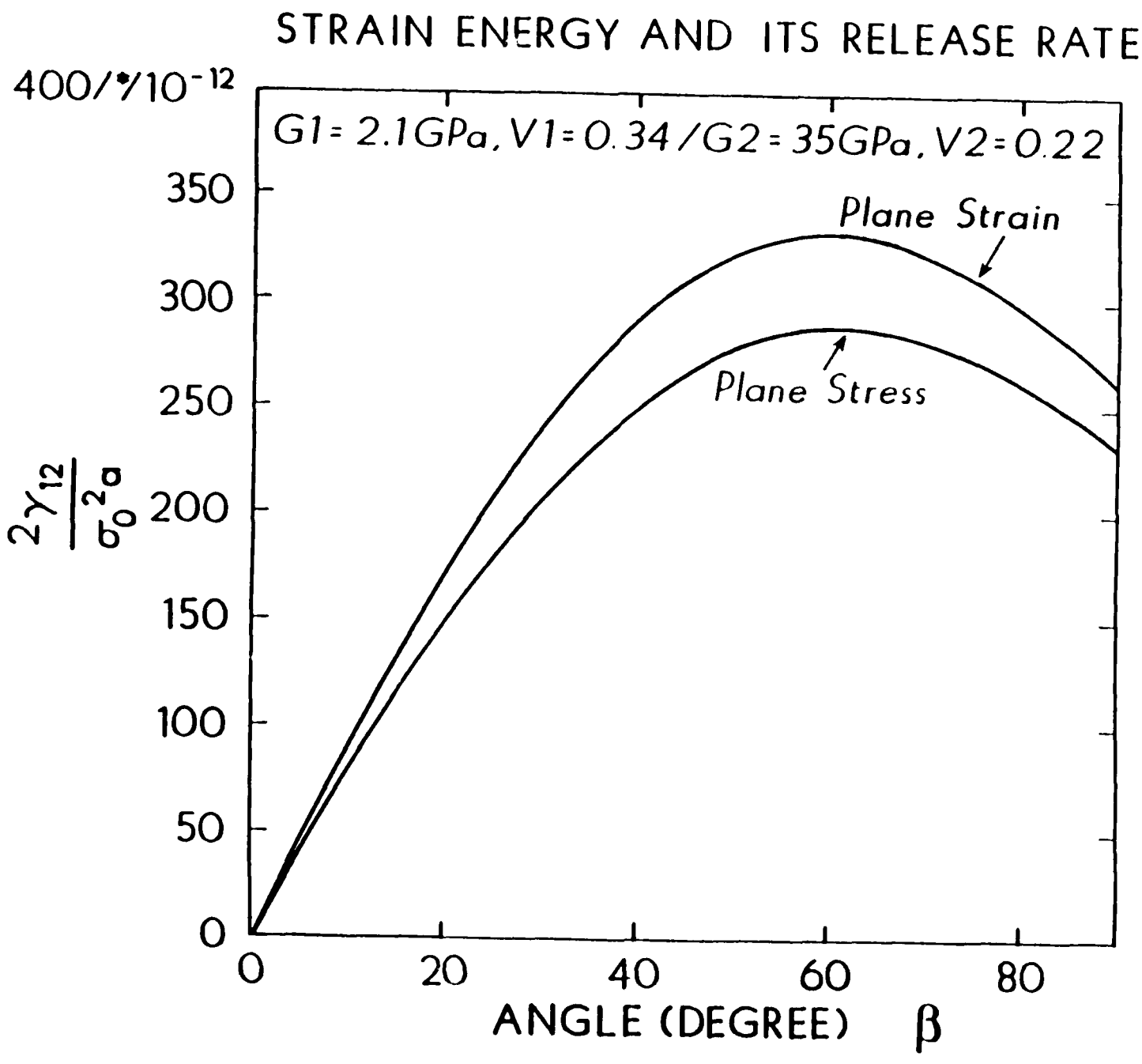

Fig. 8 **Strain energy release rate for plane stress and plane strain conditions for $\nu_1 = 0.34$, $\nu_2 = 0.22$ and $(G_2/G_1) = 16.67$**

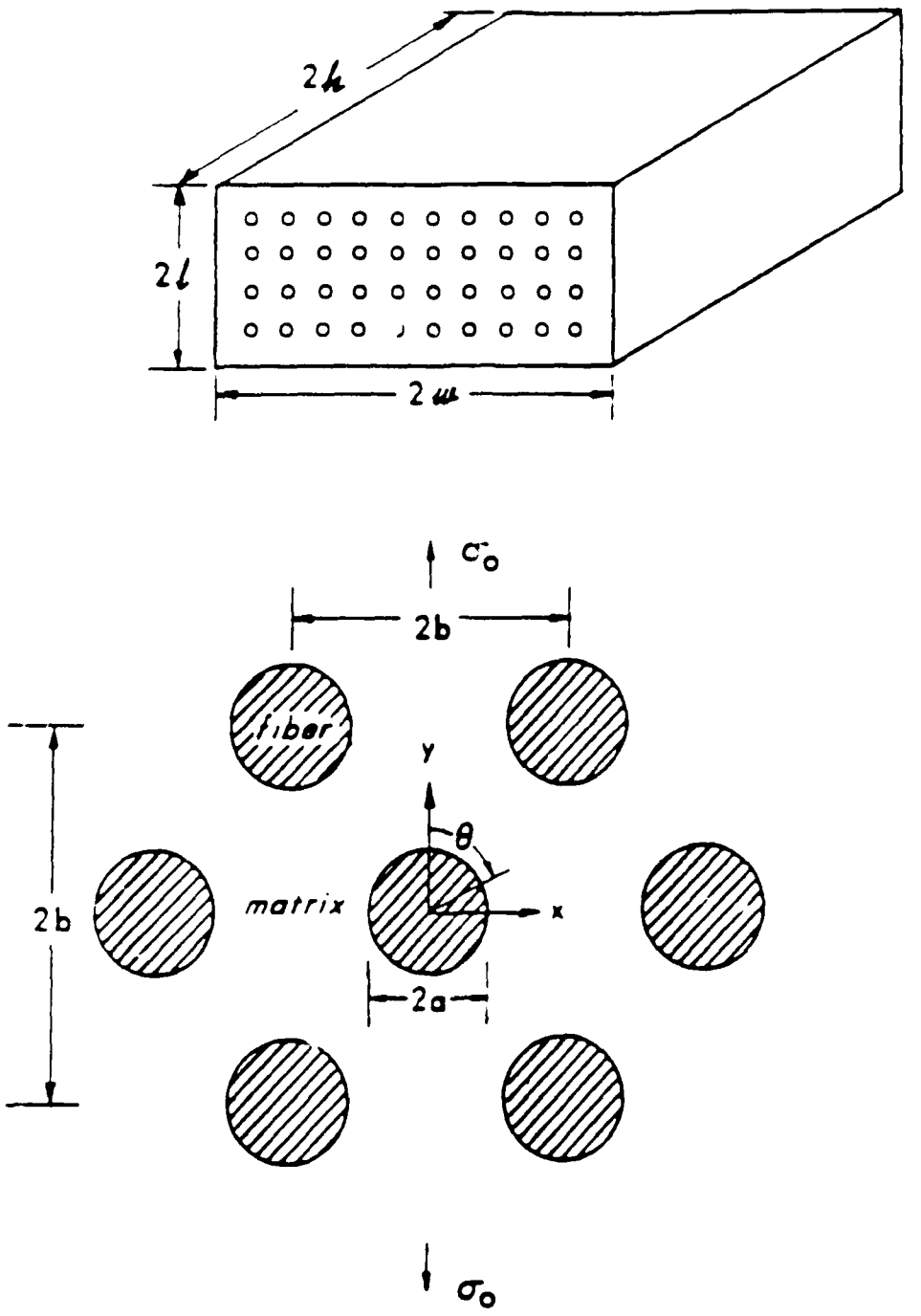

Fig. 9 Periodic array of fibers of length 2h, embedded into a matrix.

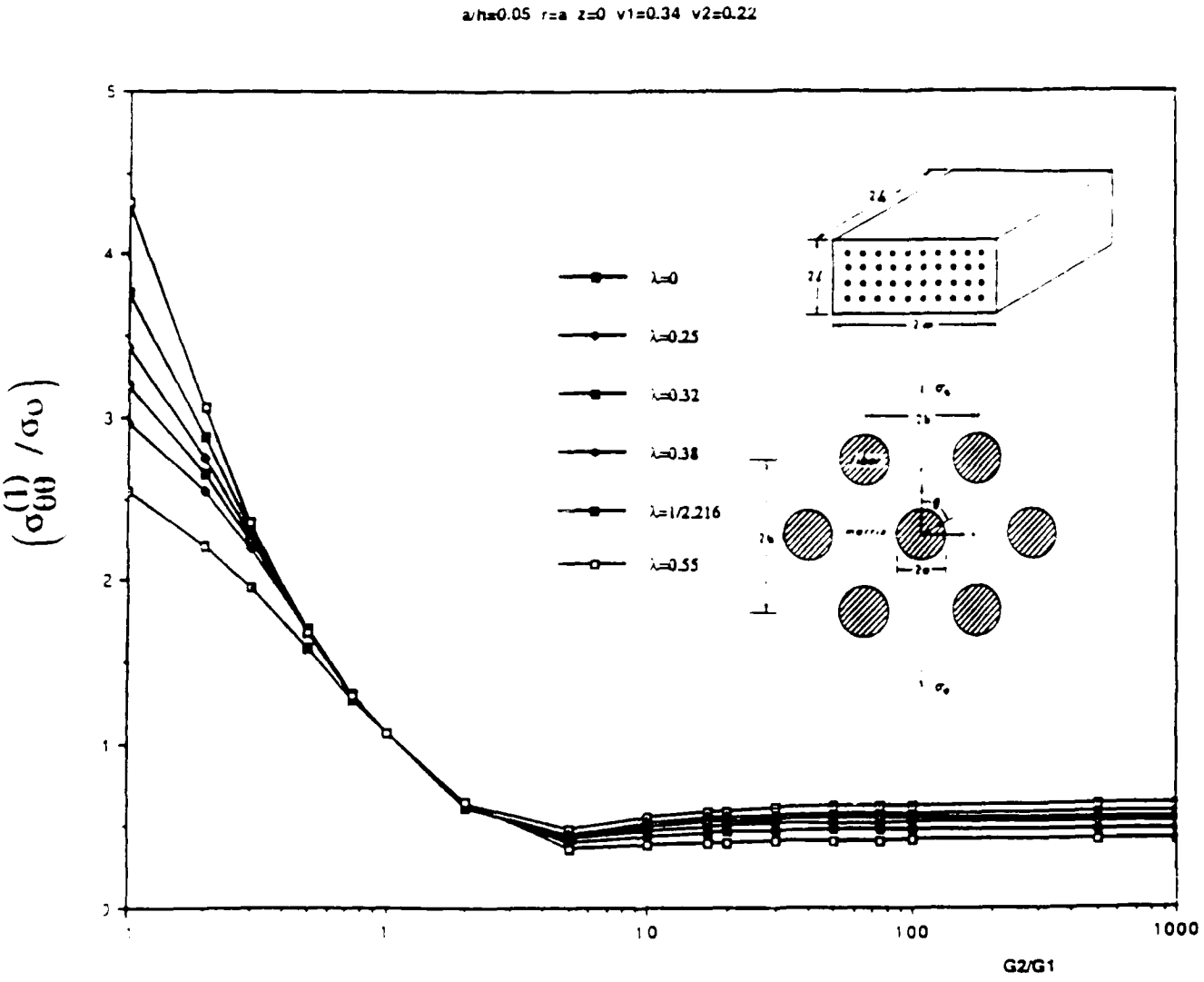

Fig. 10 Stress $\sigma_{\theta\theta}^{(1)}$ at r=a, θ=0 and for $v_1 = 0.34$, $v_2 = 0.22$, versus the ratio (G_2/G_1).

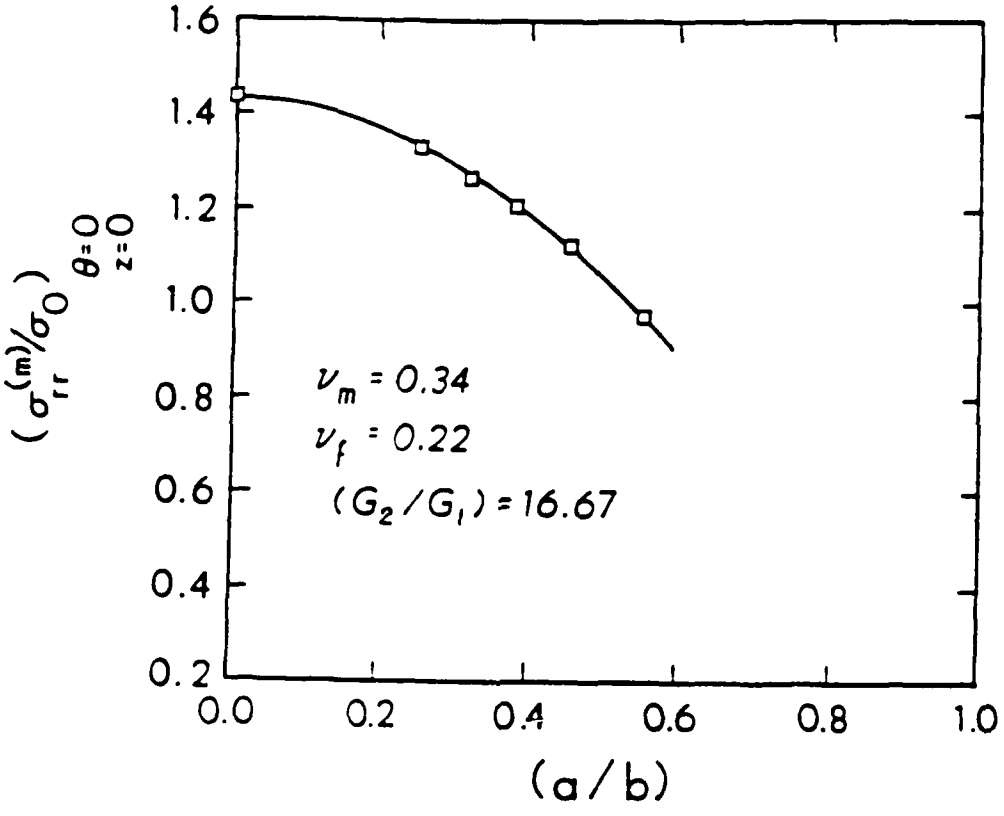

Fig. 11 Stress $\sigma_{rr}^{(1)}$ at r=a, versus a/b for $(G_2/G_1) = 16.67$ $\nu_1 = 0.34$, $\nu_2 = 0.22$

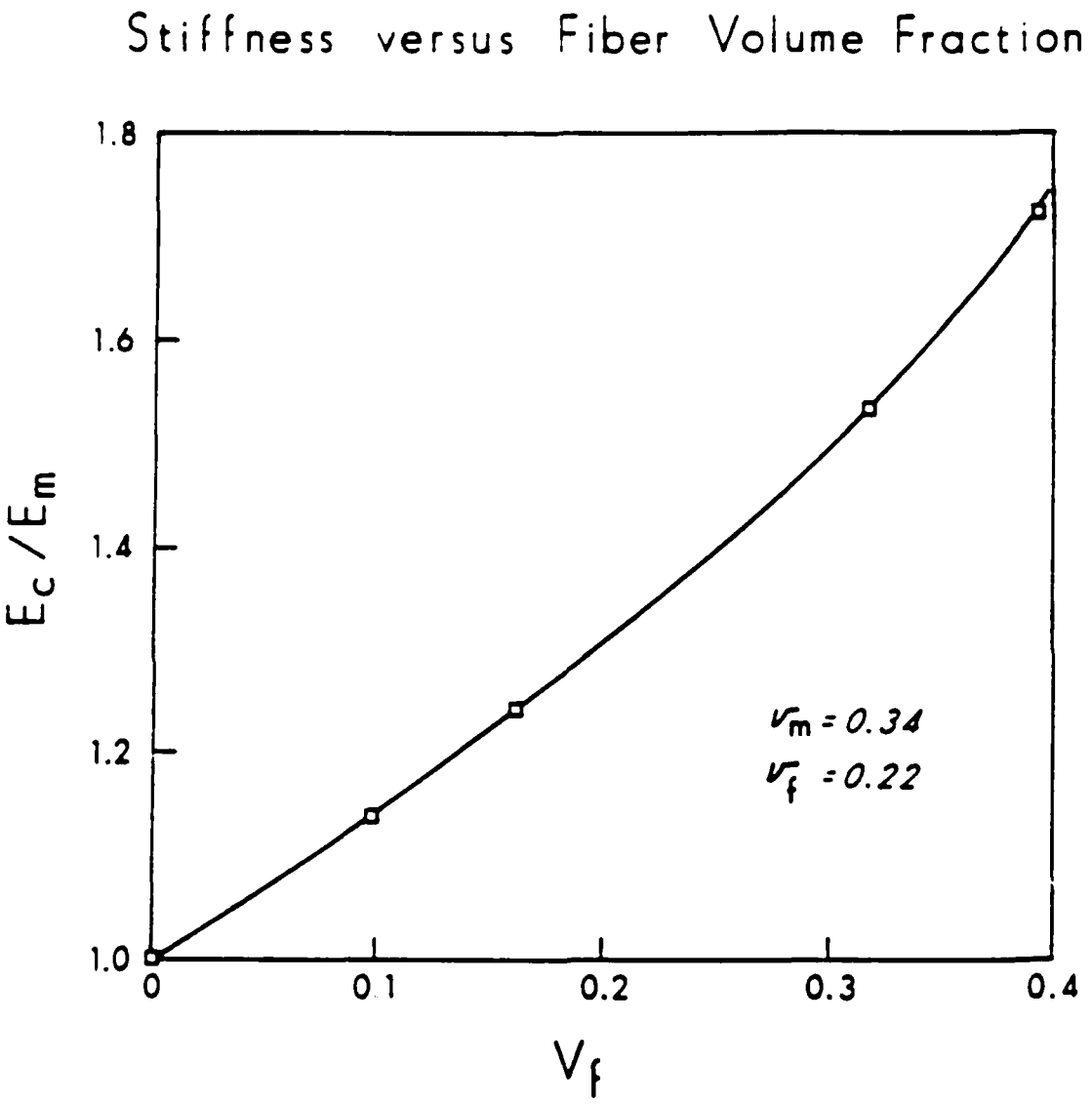

Fig. 12. Stiffness ratio versus V_f for $(G_2/G_1) = 16.67$, $\nu_1 = 0.34$ and $\nu_2 = 0.22$.